Received: 11 April 2019 | Revised: 3 September 2019 | Accepted: 7 September 2019

DOI: 10.1111/bph.14869

RESEARCH PAPER

Fenretinide treatment accelerates atherosclerosis development in apoE-deficient mice in spite of beneficial metabolic effects

Marco Busnelli[1] | Stefano Manzini[1] | Fabrizia Bonacina[1] | Sabina Soldati[2] | Silvia Stella Barbieri[3] | Patrizia Amadio[3] | Leonardo Sandrini[1,3] | Francesca Arnaboldi[4] | Elena Donetti[4] | Reijo Laaksonen[5] | Saverio Paltrinieri[2] | Eugenio Scanziani[2,6] | Giulia Chiesa[1]

[1] Department of Pharmacological and Biomolecular Sciences, Università degli Studi di Milano, Milan, Italy

[2] Department of Veterinary Medicine, Università degli Studi di Milano, Milan, Italy

[3] IRCCS, Centro Cardiologico Monzino IRCCS, Milan, Italy

[4] Department of Biomedical Sciences for Health, Università degli Studi di Milano, Milan, Italy

[5] Faculty of Medicine and Life Sciences, University of Tampere, Tampere, Finland

[6] Mouse and Animal Pathology Laboratory (MAPLab), Fondazione UniMi, Milan, Italy

Correspondence
Giulia Chiesa and Marco Busnelli, Department of Pharmacological and Biomolecular Sciences, Università degli Studi di Milano, Milan, Italy.
Email: giulia.chiesa@unimi.it; marco.busnelli@unimi.it

Funding information
European Community's Seventh Framework Programme(FP7/2012–2017), Grant/Award Number: 305739; Fondazione CARIPLO, Grant/Award Number: 2011-0645; MIUR Progetto Eccellenza

Background and Purpose: Fenretinide, a synthetic retinoid derivative first investigated for cancer prevention and treatment, has been shown to ameliorate glucose tolerance, improve plasma lipid profile and reduce body fat mass. These effects, together with its ability to inhibit ceramide synthesis, suggest that fenretinide may have an anti-atherosclerotic action.

Experimental Approach: To this aim, nine-week-old apoE-knockout (EKO) female mice were fed for twelve weeks a Western diet, without (control) or with (0.1% *w*/w) fenretinide. As a reference, wild-type (WT) mice were treated similarly. Growth and metabolic parameters were monitored throughout the study. Atherosclerosis development was evaluated in the aorta and at the aortic sinus. Blood and lymphoid organs were further characterized with thorough cytological/histological and immunocytofluorimetric analyses.

Key Results: Fenretinide treatment significantly lowered body weight, glucose levels and plasma levels of total cholesterol, triglycerides, and phospholipids. In the liver, fenretinide remarkably reduced hepatic glycogenosis and steatosis driven by the Western diet. Treated spleens were abnormally enlarged, with severe follicular atrophy and massive extramedullary haematopoiesis. Severe renal hemosiderin deposition was observed in treated EKO mice. Treatment resulted in a threefold increase of total leukocytes (WT and EKO) and raised the activated/resting monocyte ratio in EKO mice. Finally, atherosclerosis development was markedly increased at the aortic arch, thoracic and abdominal aorta of fenretinide-treated mice.

Conclusions and Implications: We provide the first evidence that, despite beneficial metabolic effects, fenretinide treatment may enhance the development of atherosclerosis.

Abbreviations: apoE, apolipoprotein E; Ctrl, control, control group; EKO, apoE knockout; Fen, fenretinide, fenretinide-treated group; HCT, haematocrit; HGB, Hb concentration; MCH, mean corpuscular Hb; MCHC, mean corpuscular Hb concentration; MCV, mean corpuscular volume; MP, monocyte progenitors; ORO, Oil Red O; PL, phospholipids; PLT, platelet; RBC, red blood cells; TC, total cholesterol; TG, triglycerides; WAT, white adipose tissue; WBC, total leukocytes, white blood cells; WT, wild-type

Marco Busnelli and Stefano Manzini equally contributed to this work.

1 | INTRODUCTION

Fenretinide is a derivative of retinoic acid, widely investigated as chemo-preventive option in different forms of cancer and as chemo-therapeutic agent in both paediatric and adult malignancies (Cooper, Reynolds, Cho, & Kang, 2017). Whereas retinoic acid and other related compounds preferentially accumulate in the liver causing hepatic toxicity with prolonged exposure, fenretinide together with its metabolites is preferentially stored in fatty tissues conferring a safer profile for this molecule (Mody & Mcilroy, 2014).

The retinoid metabolism pathway is known to play an important role in body mass regulation and adipocyte biology (Berry, DeSantis, Soltanian, Croniger, & Noy, 2012; Zizola et al., 2010) and all-*trans*-retinoic acid, the most active metabolite of retinol, has been shown to positively affect obesity and glucose homeostasis (Berry & Noy, 2009). Fenretinide improves glucose response and modulates body fat mass, at least in part through modulation of retinoid homeostasis genes (Mcilroy et al., 2013; Mody & Mcilroy, 2014). Additionally, fenretinide prevents ceramide accumulation by inhibiting dihydroceramide desaturase, which catalyses the final step of *de novo* ceramide synthesis (Bikman et al., 2012). Given the emerging role of ceramides in promoting insulin resistance and other obesity-induced metabolic alterations (Aburasayn, Al Batran, & Ussher, 2016; Petersen & Shulman, 2018), this mechanism may account for the favourable metabolic effects of fenretinide treatment (Bikman et al., 2012; Mody & Mcilroy, 2014). Further, fenretinide administration to high-fat fed mice has been shown to significantly reduce hepatic steatosis (Koh et al., 2012; Preitner, Mody, Graham, Peroni, & Kahn, 2009) and to moderately lower plasma lipids, possibly by increasing liver fatty acid oxidation (Koh et al., 2012).

All these favourable metabolic effects exerted by fenretinide suggest that this drug may be protective against cardiovascular disease. In the present study, fenretinide was administered to apolipoprotein E-deficient (EKO) mice to investigate a possible beneficial effect of this drug on the development of atherosclerosis. Although fenretinide treatment favourably affected glucose and lipid metabolism, unexpectedly it worsened atherosclerosis, possibly through a dramatic increase in the immune/inflammatory response.

What is already known

- Fenretinide, a synthetic retinoid derivative lowers body weight, reduces plasma lipids and glucose levels.
- Fenretinide inhibits the synthesis of ceramides, which are biomarkers associated to atherosclerosis development.

What this study adds

- Despite favourable metabolic effects fenretinide exacerbates plaque development in apoE knockout mice.

What is the clinical significance

- Patients enrolled in fenretinide trials must be carefully selected and monitored because of these pro-atherogenic effects.

2 | METHODS

2.1 | Animals, diet, and pharmacological treatments

Animal studies are reported in compliance with the ARRIVE guidelines (Kilkenny et al., 2010) and with the recommendations made by the *British Journal of Pharmacology*. Procedures involving animals and their care were conducted in accordance with institutional guidelines that are in compliance with national (D.L. No. 26, March 4, 2014, G.U. No. 61 March 14, 2014) and international laws and policies (EEC Council Directive 2010/63, September 22, 2010: Guide for the Care and Use of Laboratory Animals, United States National Research Council, 2011). The experimental protocol was approved by the Italian Ministry of Health (Protocollo 428/2015-PR).

Fifty apoE knockout female mice (RRID:IMSR_JAX:002052) and twenty C57BL/6 wild type (RRID:IMSR_CRL:027) aged 8 weeks were purchased from Charles River Laboratories (Calco, Italy) and housed at constant temperature and relative humidity. Mice were housed in a conventional animal facility and kept in conventional cages for small rodents (Tecniplast S.p.A., Buguggiate, Italy). Scobis Uno, a vegetable bedding made of wood particles obtained from spruce, was used. After 1 week of acclimatization, each strain of mice was randomly divided into two groups on the basis of body weight so that the distribution between the groups was similar and fed for 12 weeks a high-fat diet (adjusted calories 42% from fat, 0.2% cholesterol, from Mucedola, Settimo Milanese, Italy) without supplementation (control) or supplemented with fenretinide 0.1% w/w (Preitner et al., 2009). Mice were house three to four per cage.

2.2 | Blood and tissue harvesting

At the end of the dietary treatment, mice were anaesthetized with 2% isoflurane (Parolini et al., 2014), and blood was collected from a subset of mice, after 5-hr fast, for plasma lipid quantification, as described (Busnelli et al., 2017). In a second subset of unfasted mice, blood was collected for FACS (0.1% w/v EDTA) from the retroorbital plexus. For haematological analyses, blood was collected through cardiac puncture in 3.8% Na-citrate as described (Amadio et al., 2017).

Anaesthetized mice were killed by exsanguination as a result of perfusion with PBS. Aorta was then rapidly harvested as described (Parolini et al., 2017), longitudinally opened and pinned flat on a black wax surface in ice-cold PBS and then photographed unstained for plaque quantification (see below).

Heart, liver, lungs, abdominal white adipose tissue (WAT), kidneys, skin, spleen, and bone marrow were harvested. Liver and WAT were snap-frozen in liquid nitrogen for subsequent molecular analyses. All listed tissues were processed for subsequent histological or cytological analyses.

The experimenters performing all the procedures described below were blinded to the treatments the mice had received.

2.3 | Plasma measurements and glucose tolerance test

Plasma total **cholesterol** (TC), triglycerides (TG) and phospholipids (PL) were measured with enzymatic methods and lipid distribution among lipoproteins was analysed by FPLC (Marchesi et al., 2011). The following cytokines/chemokines were measured in plasma: Il-1β, Il-2, Il-4, Il-5, Il-6, Il-10, Il-12(p70), Il-17, Ifn-γ, Tnf, Ccl2/Mcp-1, and Ccl5, using the Mouse Magnetic Luminex Assay. Cytokine/chemokine measurements were outsourced to a certified laboratory (Labospace Srl, Milan, Italy).

For the glucose tolerance test, after 10 weeks of treatment, mice were fasted for 5 hr and then injected with 2 $g \cdot kg^{-1}$ glucose via intraperitoneal injection of 20% w/v sterile glucose solution in PBS. Glucose levels were determined as described previously (Lachance et al., 2013).

2.4 | Functional fibrinogen

Plasma fibrinogen was assayed by Clauss method according to manufacturer's instructions, as previously described (Amadio, Tarantino, Sandrini, Tremoli, & Barbieri, 2017). Briefly, plasma samples were diluted 1:10 in imidazole buffer (imidazole 0.34%, NaCl 0.6%, sodium citrate 0.15%, HCl 0.14%, sodium azide 0.33%; pH 7.4). Two-hundred microlitres of each diluted plasma sample were prewarmed at 37°C for 4 min, and then clot formation was promoted by the addition of 100 µl of liquid stable thrombin reagent (100 $U \cdot ml^{-1}$). The time taken for the clot to form is directly proportional to fibrinogen concentration present in the samples analysed (Mackie et al., 2003).

2.5 | Blood and bone marrow cytology

2.5.1 | Sampling

At sacrifice, blood was collected from the heart and immediately placed in 0.5 ml tubes containing EDTA, filled to their maximum capacity. Anti-coagulated blood was stored at room temperature and transported to the laboratory to be processed within 4 hr from sampling as described below.

Bone marrow was collected from the femur using a 24G syringe needle through the needle capillary technique: The femur was removed at necropsy and longitudinally split using a bone cutter, and the needle was inserted in the bone marrow cavity. Once removed, the content of the needle was sprayed on a glass slide using a 1 ml syringe, and the needle itself was rolled on the slide to smear either the material contained in the needle or the small drops of tissues remained in the outer surface of the needle.

2.5.2 | Haematology and bone marrow cytology

Routine haematology was performed on whole blood collected in EDTA using a laser-based cell counter (Sysmex XT-2000iV) validated in mice (Mathers et al., 2008). Samples with evident clots were excluded from the haematological analysis. The following parameters were evaluated: erythrocyte number (RBC), Hb concentration (HGB), haematocrit (HCT), mean corpuscular volume (MCV), mean corpuscular Hb (MCH), mean corpuscular Hb concentration (MCHC), platelet number (PLT) and the number of total leukocytes (WBC) consisting of neutrophils, lymphocytes, monocytes, eosinophils and basophils. The differential leucocyte counts provided by the instrument were verified through microscopic evaluation on May Grünwald Giemsa stained smears. During microscopic evaluation, particular attention was paid to the differentiation of mature (segmented) neutrophils and immature (band) neutrophils and to any possible morphological abnormality of erythrocytes, leukocytes, and platelets.

Bone marrow smears were stained with May Grünwald Giemsa and a 500 nucleated-cell count was microscopically performed. The following parameters were recorded: myeloid:erythroid (M:E); number of cells belonging to the proliferative (P) pool (composed by blasts able to divide) or to the maturation (M) pool, in order to calculate, for each cell population, the P:M ratio, and the percentage of precursors on the total number of cells belonging to each cell lineage (%EP = percentage of erythroid precursors and %MP = percentage of myeloid precursors); percentage of lymphocytes (%L) and plasma cells (%PL) on the total number of counted cells. Any possible abnormal morphology of cells of both proliferative and maturation pool was also recorded.

2.6 | FACS analyses

2.6.1 | Flow cytometry

All fluorochrome-conjugated antibodies were used at 1:100 dilutions unless otherwise specified. Samples were acquired with Novocyte 3000 (ACEA Biosciences) and analysed with Novoexpress software.

2.6.2 | Blood immunophenotyping

The immuno-related procedures used comply with the recommendations made by the *British Journal of Pharmacology*. Fifty microlitres of blood were stained with the mix of fluorochrome-conjugated antibodies prepared in PBS containing 2% FBS and 2-µM EDTA (MACS buffer) at RT for 30 min in the dark. Following staining, red blood cells were lysed and fixed for 20 min at RT, washed twice and resuspended with MACS buffer and analysed immediately.

2.6.3 | Spleen and bone marrow cells immunophenotyping

Spleens were weighed and then immune cells were isolated. A uniform cell suspension was prepared by the spleens through a 70 µm cell strainer; after red blood cell lysis (red blood cell lysis buffer), cells were spun down at 600× *g* for 5 min suspended in MACS buffer for cell counting.

Bone marrow cells were isolated by flushing femurs with MACS buffer. Cells were then dispersed with a 5 ml syringe and pass through a 70 μm cell strainer and likewise suspended for counting.

A cell suspension of 100 μl of cells from spleen and bone marrow was stained with a mix of superficial fluorochrome-conjugated antibodies mix prepared in MACS buffer at 4°C for 30 min in the dark. Cells were washed twice and resuspended with MACS buffer if analysed immediately.

Antibodies for the following markers were used to identify immune populations: In the blood, CD45 was used for identification of total leukocytes, CD3 for T lymphocytes, CD19 for B lymphocytes, CD11b for cells of myeloid lineage, Ly6G for neutrophils, CD115 for monocytes, and Ly6C for monocyte subsets, being highly expressed on activated ($Ly6C^{hi}$) and low expressed on resting monocytes ($Ly6C^{lo}$). In the spleen, in addition of markers used in the blood, macrophages were identified as CD11b+F4/80+, while dendritic cells as CD11c+MHCII+. Detailed gating strategy can be found in Figures S10–S12.

2.7 | Platelet/leukocyte aggregates

Twenty microlitres of whole blood were stimulated at RT for 5 min with 5 μM ADP, then 200 μl of cell blood lysis buffer (BD Biosciences) were added for 15 min, and then samples were stained with saturating concentrations of anti-CD45 (leukocytes), anti-CD41 (platelets), and anti-CD14 (monocytes) or anti-Lys6G (neutrophils) or isotype controls at RT for 30 min in the dark. Aggregates were counted by flow FACS "Novocyte3000." A minimum of 5,000 events was collected in the CD14+ or Lys6G+ gate as previously described (Sandrini et al., 2017).

2.8 | En face analysis of the aorta, aortic sinus histology, and immunohistochemistry

2.8.1 | En face

Aorta images were captured with a stereomicroscope-dedicated camera (IC80 HD camera, MZ6 microscope, Leica Microsystems, Germany) and analysed with ImageJ image processing programme (RRID: SCR_003070; Schneider, Rasband, & Eliceiri, 2012). Two independent operators, blinded to the dietary treatments, quantified atherosclerosis extent as percentage of area covered by plaque.

2.8.2 | Aortic sinus histology

Hearts were removed, fixed in 10% formalin, and processed as previously described (Vik et al., 2013). Serial cryosections (7 micron thick) of the aortic sinus were cut and stained with haematoxylin and eosin (H&E; Parolini et al., 2014) to detect plaque area, calculated as the mean area of those sections showing the three cusps of the aortic valves. On the same sections, the area occupied by foam cells and necrotic core was measured. Adjacent slides were stained with Sirius red to determine collagen deposition, with Oil Red O to detect intraplaque neutral lipids, and with Perls' iron staining to highlight the presence of hemosiderin.

Immunohistochemical stainings were used to detect intraplaque macrophages and erythrocytes. Macrophages were identified using a rat monoclonal IgG2a (clone M3/38) against galectin-3 (Mac-2, 1:1,000 dilution). Erythrocytes were detected with a rat monoclonal IgG2b (clone TER-119) against Ly76, (1:100 dilution). In both immunohistochemical stainings, primary antibodies were diluted in PBS 1× with an incubation of 1 hr at room temperature (RT). In negative controls, primary antibodies were omitted (Figure S13). Detection was performed using the ImmPRESS reagent kit. The ready-to-use secondary goat antibody (anti-rat IgG), conjugated with HRP micropolymers, was used following manufacturer's instructions, with an incubation of 20 min at RT. 3,3′-Diaminobenzidine was used as the chromogen, and the sections were counterstained with Gill's haematoxylin.

The Nanozoomer S60 (Hamamatsu Photonics, Japan) scanner was used to acquire digital images that were subsequently processed with the NDP.view2 software (Hamamatsu Photonics, Japan). Two blinded operators to dietary treatments quantified histological and immunohistochemical results (Alexander et al., 2018).

2.9 | Liver, abdominal WAT, spleen, and kidney histology

Formalin-fixed organs/tissues were dehydrated in a graded scale of ethanol and paraffin embedded (Howard et al., 2018). Sections (4 micron thick) were cut and stained with H&E. Perls' iron staining was used to confirm the presence of hemosiderin in kidney and liver. All histological and histochemical features were assessed by a veterinary pathologist blinded to treatments.

2.10 | Skin histology

At sacrifice, skin biopsies were excised from the thoracic region, dissected in smaller fragments, and processed for light microscopy analysis. For each animal, skin biopsies were divided in both fragments of 5 × 5 mm and 2 × 2 mm.

Fragments of 5 × 5 mm were immersion-fixed in 4% paraformaldehyde buffered with PBS 0.1 M (pH 7.4) for 5 hr at room temperature, dehydrated with ethanol, and paraffin embedded. Four-micrometre serial sections were stained with H&E to observe skin morphology at the structural level.

For transmission electron microscopy, skin specimens of 2 × 2 mm were processed as previously described (Arnaboldi et al., 2015). Semithin sections, 2 μm thick, were stained with toluidine blue.

All sections were observed with a Nikon Eclipse E600 microscope equipped with a Nikon digital camera DXM1200 (Nikon, Tokyo, Japan).

2.11 | RNA extraction and cDNA synthesis

Total RNA was isolated from mouse tissues and extracted as previously described (Manzini et al., 2018). RNA was quantified and purity was checked, and 1-μg RNA was retrotranscribed to cDNA, as described (Manzini et al., 2015). Possible gDNA contamination was ruled out by

running a PCR on 20 ng of cDNA/RNA with a primer pair producing two amplicons of different size on cDNA (193 bp) and gDNA (677 bp). Conditions were as follows: 95°C for 3 min, followed by 35 cycles of 30 s at 95°C, 30 s at 58.5°C, and 45 s at 72°C for 45 s, followed by a final amplification step of 5 min at 72°C, with primers mmu_Srp14_f: 5′-GGAGGCTTCTGCTGACGGCG-3′ and mmu_Srp14_r: 5′-GGGCTCGAGGCCCTCCACA-3′.

2.12 | Quantitative PCR

Twenty nanograms of cDNA were used as template for each qPCR reaction, performed on a CFX Connect thermal cycler with iTAQ Universal Sybr Green Supermix. Standard fast cycling conditions were used, with 300-nM primer pairs detailed in Table S1. A final melting curve analysis was always performed. Fold changes relative to control group were calculated with the ΔΔCt method (Livak & Schmittgen, 2001). The gene cyclophilin A (Ppia) was used as reference gene.

2.13 | Data and statistical analyses

The data and statistical analysis comply with the recommendations of the *British Journal of Pharmacology* on experimental design and analysis in pharmacology (Curtis et al., 2015). Statistical analyses are detailed for each individual analysis in the appropriate figure or table caption. When ANOVA was used, post hoc tests were run only if F achieved $P < 0.05$ and there was no significant variance inhomogeneity. The threshold for statistical significance was set at $P = 0.05$. Analyses were performed with R, version 3.3.3 (R Core Team, 2017), with packages reshape (Wickham, 2007) and PMCMR for Kruskal–Wallis Conover's post hoc (Pohlert, 2014).

2.14 | Materials

The following where used: - animal bedding (Scobis Uno) and diets (Chow diet; COD RF-21 & adjusted calories 42% from fat, 0.2% cholesterol) from Mucedola, Settimo Milanese, Italy. Anti-mouse antibodies: CD45 FITC-conjugated COD:553079 (RRID AB_394609), CD3 PerCP-Cy5.5-conjugated COD:560527 (RRID AB_1727463), CD19 PE-CF594-conjugated COD:562329 (RRID AB_11154580), CD11b APC-Cy7-conjugated COD:561039 (RRID AB_2033993), CD115 PE-conjugated COD:565249 (RRID AB_2739132), Gr-1(Ly6C/Ly6G) BV605-conjugated COD:563299 (RRID AB_2738126), F4/80 Af647-conjugated COD:565854 (RRID AB_2744474), MHCII BV650-conjugated COD:563415 (RRID AB_2738192), CD11c BV786-conjugated COD:563735 (RRID AB_2738394), FITC rat anti-mouse CD41 COD: 553848 (RRID AB_395085), Anti-TER119 antibody–COD: 550565 (RRID AB_393756), PE rat anti-mouse CD45 COD: 561087 (RRID AB_10563412) and PE rat anti-mouse CD14 COD: 553440 (RRID AB_395022) from BD bioscience, Franklin Lake, USA.; Anti-galectin-3 antibody COD: CL8942 (RRID AB_10060357) from Cedarlane, Ontario, Canada, biotin anti-mouse Ly-6G antibody COD: 127603 (RRID AB_1186105) and anti-mouse CD206 PECy7-conjugated COD: 25-2069-41 (RRID AB_2573425). Assay kits:- cholesterol assay COD:CP A11 A01634 and triglycerides assay COD:CP A11 A01640 from ABX Diagnostics, Montpellier, France; high capacity cDNA reverse Transcription kit COD:4368814 from Applied Biosciences, Foster City, USA; phospholipids assay from B.L. Chimica, Concorezzo, Italy; iTAQ universal Sybr green supermix from Bio-Rad, Segrate, Italy; Anti-mouse/rat Foxp3 staining set APC COD:77–5775-40 (RRID AB_469981) and Foxp3/transcription factor staining buffer set from eBioscience, Waltham, USA; Clauss fibrinogen from Futura System, Roma, Italy; NucleoSpin RNA extraction kit from Macherey-Nagel, Duren, Germany; PCR primer from MWG, Ebersberg, Germany and Cytokine detection system, Cat. No. LXSAMSM from R&D Systems, Minneapolis, USA. Chemicals, reagents and drugs:- Mayer's haematoxylin, Eosin Y alcoholic solution, Gill's haematoxylin, Perls COD. 04-180807 from Bio-Optica, Milano, Italy; 3,3′-Diaminobenzidine (DAB) from Biocare medical, Pacheco, USA; 1-step fix/lyse solution COD: 00-5333-54, and Red blood cell lysis buffer COD: 00-4300-54 from eBioscience, Waltham, USA; Durcupan from Fluka, Milano, Italy; Tissue-Tek® O.C.T.™ from Sakura Finetek, Alphen aan den Rijn, The Netherlands; Isoflurane from Merial Animal, Woking, UK; all other chemicals from Sigma-Aldrich, St Louis, USA. Staining Kits: Sirius Red Picrate COD: 04–121873 from Bio-Optica, Milano, Italy and anti-rat IgG ImmPRESS reagent kit, COD: MP-7444 (RRID AB_2336530) from Vector Laboratories, Peterborough, UK. Mouse cages from Tecniplast, Buguggiate, Italy and blood sampling cytology tubes, Miniplast from LP Italiana, Milano, Italy.

2.15 | Nomenclature of targets and ligands

Key protein targets and ligands in this article are hyperlinked to corresponding entries in http://www.guidetopharmacology.org, the common portal for data from the IUPHAR/BPS Guide to PHARMACOLOGY (Harding et al., 2018), and are permanently archived in the Concise Guide to PHARMACOLOGY 2015/16 (Alexander, Christopoulos, et al., 2017; Alexander, Fabbro, et al., 2017).

3 | RESULTS

3.1 | Fenretinide treatment reduced weight gain without lowering food intake

At randomization (Day 0), the body weight of the two EKO groups was comparable, as well as that of WT groups: EKO-Ctrl mice weighed 19.4 ± 0.9 g and EKO-Fen 19.4 ± 0.7 g; the weight of WT-Ctrl was 17.2 ± 0.9 g and that of WT-Fen was 17.4 ± 1.1 g. The growth curves of the four groups during the experimental study are shown in Figure 1a. Fenretinide treatment reduced the weight gain of both EKO and WT mice, with differences that reached statistical significance versus their respective controls starting from Day 52 and Day 61 of treatment, respectively. At sacrifice, the mean body weight of EKO-Fen was 10.0% lower than that of EKO-Ctrl and WT-Fen mice weighed 16.5% less than WT-Ctrl. This reduction was paralleled by a

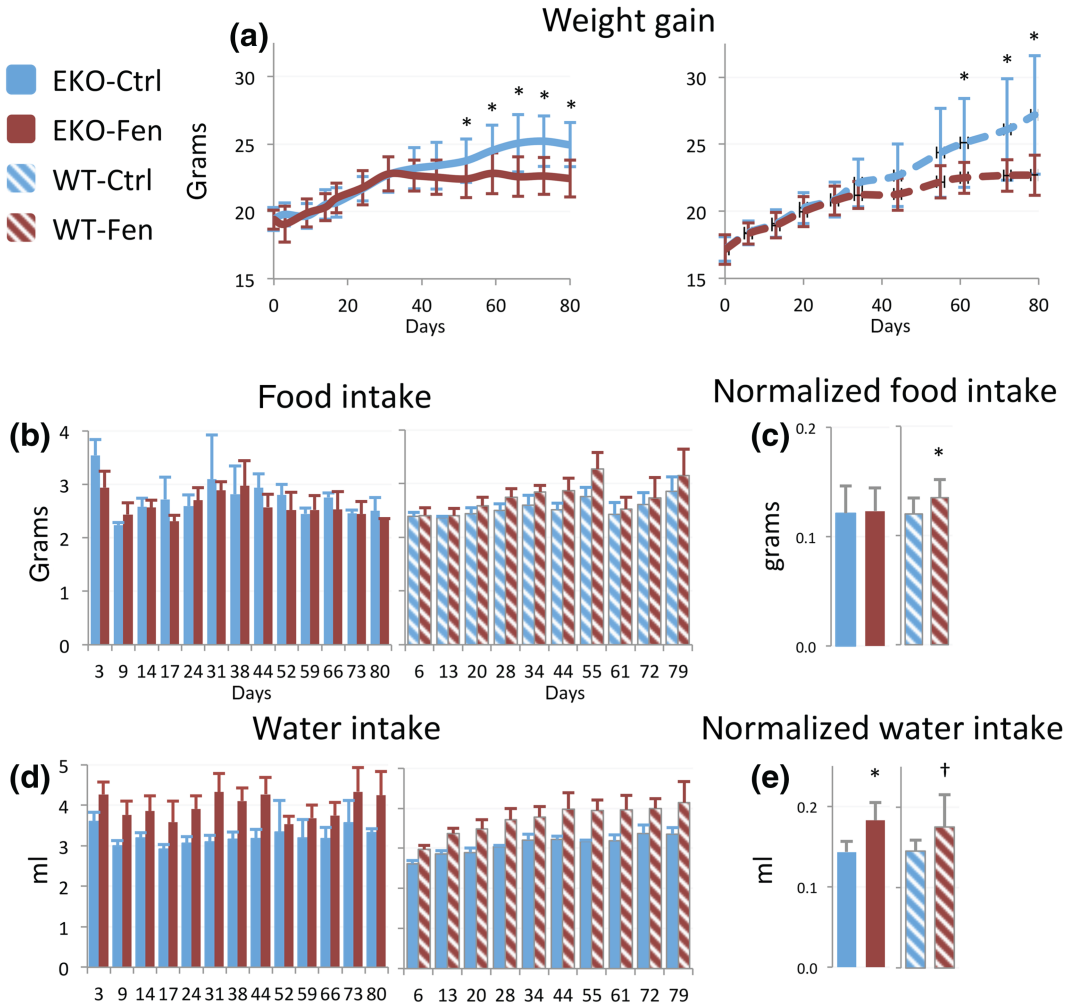

FIGURE 1 The weight of mice (n = 20 for EKO; n = 10 for BL/6) was monitored two to three times a week for a period of 12 weeks total. (a) Average weight is plotted and shown within ±1 *SD* for either EKO (left) or BL/6 (right). Weight differences started to become steadily statistically significant starting from Day 52 for EKO and Day 61 for BL/6. Likewise, food and water intake were monitored per cage (mice were housed three to four per cage) and normalized to the number of animals in each cage. Average values and *SD* are charted for each time point (b, d). For each time point, average intakes were normalized to the average weight of mice in each cage; the average of all measurements is charted for food (c, **P***0.05** < 0.05,*F* value 12.88) and water (e, **P* < 0.05, *F* value 76.46; †*P* < 0.05, *F* value 39.00). Unpaired two-tailed Student's *t*-`test was used to test mean differences at each time point (a), and significant differences are indicated by an asterisk. Repeated-measures ANOVA was used to test for differences between groups throughout the entire duration of the study (b, d are graphically summarized in c, e, respectively). Data are shown ±*SD*

strong decrease of WAT. Indeed, the abdominal WAT, used as a proxy, showed a strong reduction in both WT-Fen (−58.1%) and EKO-Fen (−74.8%) mice (Figure S1).

Food and water intake were periodically monitored (Figure 1b,d). Daily food intake, normalized to body weight, was comparable between EKO-Ctrl and EKO-Fen (Figure 1c). Conversely, food intake of WT-Fen mice was about 12% higher than that of WT-Ctrl mice (Figure 1c).

From the beginning of the study, an increased water intake was recorded in fenretinide-treated mice (Figure 1d), resulting in an higher normalized daily water intake in both fenretinide-treated groups (Figure 1e).

3.2 | Fenretinide treatment lowered plasma glucose levels in EKO mice

At baseline, after 5-hr fast, significantly lower glucose levels were detected in EKO-Fen mice compared with EKO-Ctrl mice (Figure 2a). During the glucose challenge, the mean glucose concentrations were lower in treated than in control mice, but statistical significance was not attained. This also applied when considering the AUC (Figure 2b). At the end of the challenge, that is, at 100 min, and at the regaining of baseline at 125 min, glucose levels returned to be significantly lower in EKO-Fen than in EKO-Ctrl mice, consistent with pre-challenge values.

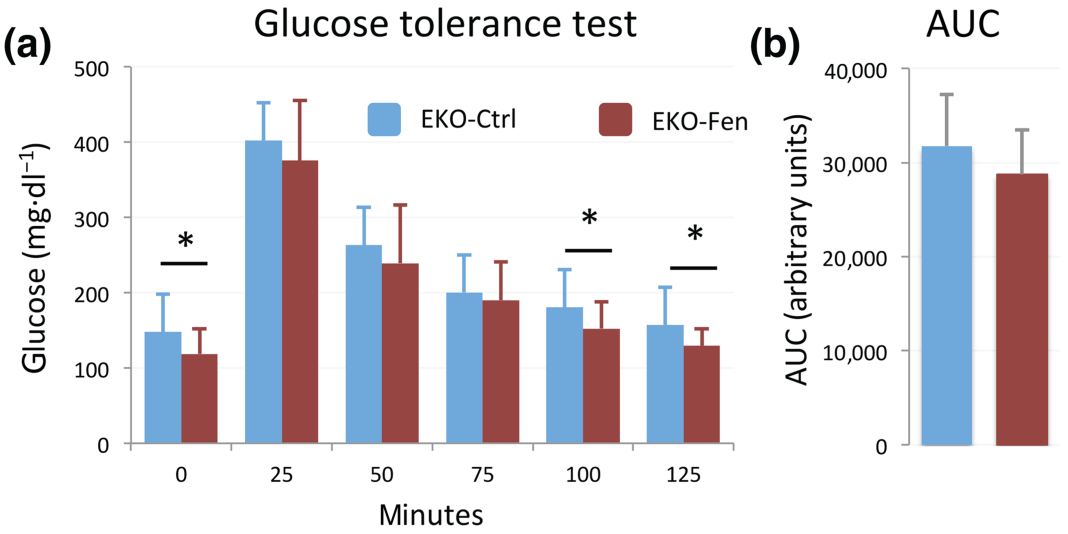

FIGURE 2 After an intraperitoneal injection of 2 g·kg^{-1} glucose (n = 16 randomly chosen EKO mice per group), glycaemia has been monitored at intervals of 25 min, up to 125 min total. Glucose concentration as function of time is charted. *P < 0.05 (a). Measurements of AUCs are shown in (b), in arbitrary units. Repeated-measures ANOVA was used to test for statistically significant differences (a, F score 3.66) and by unpaired two-tailed Student's t test (b). Data are shown ±*SD*

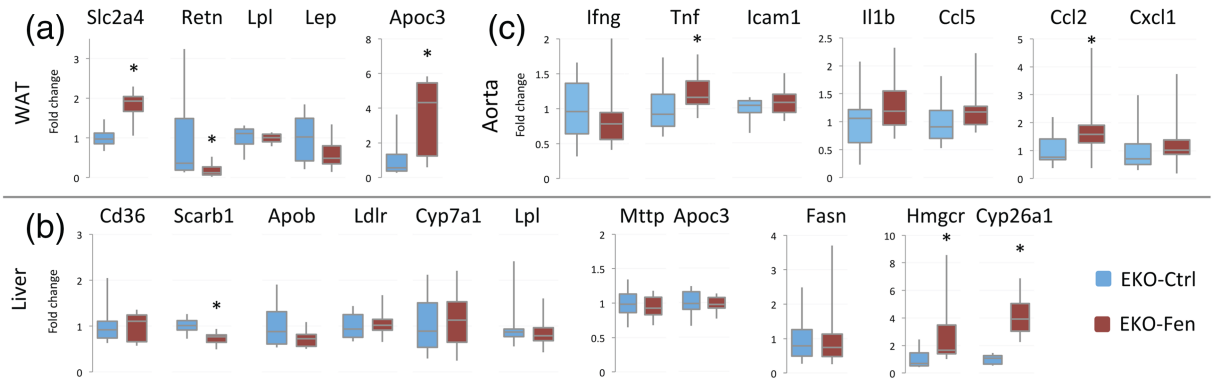

FIGURE 3 Box plots of gene expression in the abdominal white adipose tissue (a), liver (b), and aorta (c) are shown (n = 12 for a and b and n = 15 for c, randomly chosen EKO mice per group; each sample was run in triplicate). (a) Fold changes of genes quantified in the abdominal white adipose tissue, relative to EKO-Ctrl group, are charted. (b) Fold changes of hepatic genes, relative to EKO-Ctrl group, are charted. (c) Fold changes of aortic genes, relative to EKO-Ctrl group, are charted. Statistically significant differences were determined by unpaired two-tailed Student's t-test. *P < 0.05. The upper and lower ends of the boxes indicate the 25th and 75th percentiles, respectively. The length of the box shows the interquartile range within which 50% of the values are located. The solid grey lines denote the median

GLUT-4 (Slc2a4 gene) expression was almost twofold higher in the WAT of EKO-Fen, with respect to EKO-Ctrl (Figure 3a). Additionally, Resistin (Retn gene) expression in WAT was almost fivefold decreased in EKO-Fen with respect to EKO-Ctrl (Figure 3a).

Histological features in WAT were not significantly different between groups. In the liver, a very large decrease in the amount of glycogen stored in the cytoplasm of hepatocytes was observed in EKO-Fen compared to EKO-Ctrl (Figure S2); a mild decrease was observed in WT-Fen mice compared to WT-Ctrl (Table S2).

3.3 | Fenretinide reduced plasma lipid concentrations in EKO

At the end of treatment, plasma lipid concentrations were measured in EKO mice after 5-hr fasting. Fenretinide treatment strongly lowered plasma lipid levels (Figure 4a). Total cholesterol (TC) levels were significantly reduced by 20.1% compared to control and this decrease was mostly attributable to a cholesterol reduction in the LDL fraction, as assessed by FPLC analysis (Figure 4b). Triglyceride (TG) levels were also dramatically reduced (Figure 4a). This reduction affected all lipoprotein classes (Figure 4c). Lastly, phospholipids also showed a significant reduction with fenretinide treatment (−20.1%; Figure 4a).

Histological examination of liver showed that the high-fat diet in EKO-Ctrl mice caused steatosis, which was severely lowered by fenretinide treatment (Figure S2). Steatosis was not observed in WT-Ctrl and WT-Fen mice (Table S2).

In the liver of treated animals, fenretinide caused a threefold induction of Hmgcr and a small, but significative down-regulation of SR-B1 (Scarb1 gene; Figure 3b). No significant changes in the expression of

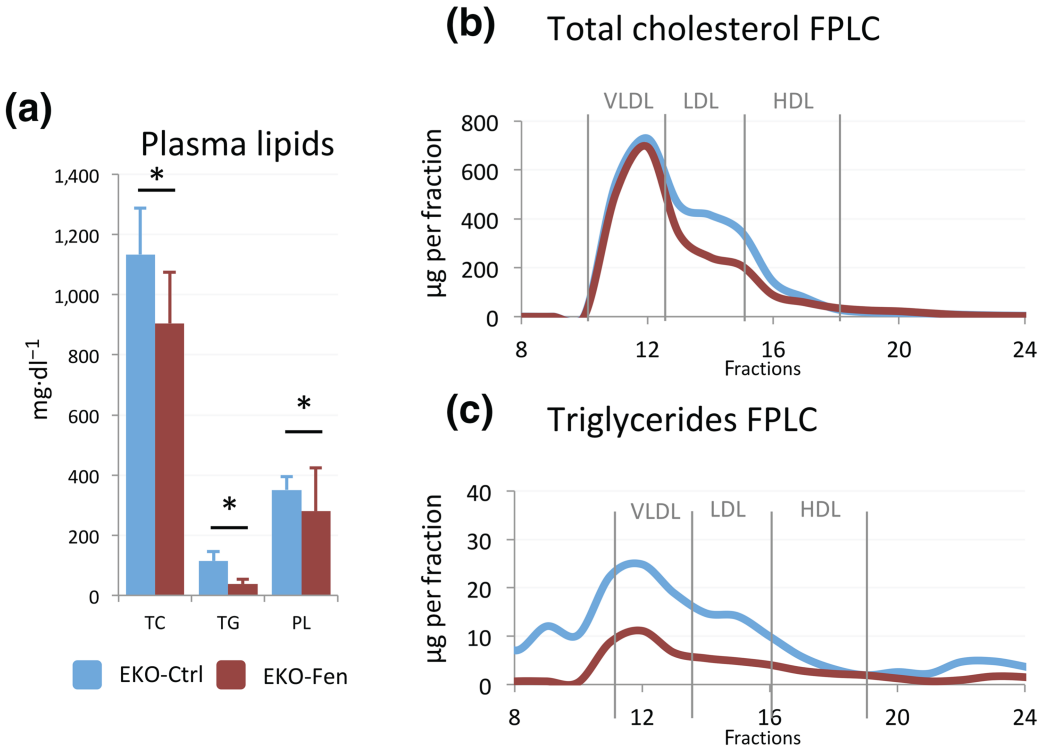

FIGURE 4 Total cholesterol (TC), triglyceride (TG), and phospholipid (PL) levels (n = 20, each sample was assayed in duplicate), quantified after 5-hr fasting, are shown. *P < 0.05 (a). TC and TG distribution among plasma lipoproteins by FPLC is shown in (b) and (c), respectively. Each profile was obtained from pooled plasma of all mice within each experimental group (n = 20). Statistically significant differences were determined by unpaired two-tailed Student's t-test. Data are shown ±SD

the other investigated genes relevant to lipid/lipoprotein metabolism were observed (Figure 3b).

3.4 | Fenretinide dramatically worsened atherosclerosis development in EKO mice

Atherosclerotic plaque development was measured on aortas cut lengthwise, as percentage of area occupied by plaques, in the three aortic districts. In each segment, plaque development in fenretinide-treated mice was significantly higher with respect to control mice (Figure 5a). Specifically, plaque development was higher in EKO-Fen with respect to EKO-Ctrl at the aortic arch, thoracic and abdominal aortas, respectively (Figure 5b).

Plaque extent was further quantified at the aortic sinus (Figure 5c, d) and provided similar results: Plaque area was increased by 50.8% in EKO-Fen with respect to EKO-Ctrl.

Plaques of EKO-Fen were characterized by an increased collagen content and a larger necrotic core, in terms of both absolute values and relative amounts (Table 1 and Figure S3). The area occupied by macrophages, foam cells and neutral lipids was instead comparable between EKO-Fen and EKO-Ctrl, thus resulting in lower relative amounts of these plaque components (Table 1 and Figure S3) as treated mice developed larger plaques.

The presence of hemosiderin in plaques was significantly increased in EKO-Fen versus EKO-Ctrl, whereas scattered erythrocytes were found in the same amounts in plaques of both experimental groups (Figure S4 and Table S3). In one third of EKO-Fen, elongated structures strongly positive for erythrocyte immunostaining, reminiscent of thrombi-derived Lambl's excrescences, were visible within the lumen of the aortic sinus (Figure S5).

3.5 | Fenretinide dramatically increased blood leukocytes and affected erythrocyte and platelet counts

Total white blood cell counts were significantly increased upon fenretinide treatment, in both EKO and WT mice (Figure 6a). Monocytes and eosinophils were unchanged in control and treated mice, but lymphocyte counts were significantly higher, over twofold increased, in both EKO and WT mice (Figure 6b). Also, neutrophils were increased upon fenretinide treatment, even if the difference was significant only in WT mice (Figure 6b).

Plasma IL-6 concentration was significantly increased in EKO-Fen mice versus EKO-Ctrl. A moderate elevation of IL-10 was also observed in treated mice, but the levels remained very low (Table S4). Fenretinide treatment also increased Tnf and Ccl2 expression in the whole aorta (Figure 3c).

Erythroid parameters decreased in treated animals either in EKO (RBC −25.0%, HGB −19.8%, HCT −6.7%) or in WT mice (RBC −11.3%, HGB −13.6%, HCT −10.0%). All the differences above were statistically significant, except for the HCT of EKO mice (Figure 6c). In EKO-Fen mice, RBC were macrocytic (MCV +19.0%)

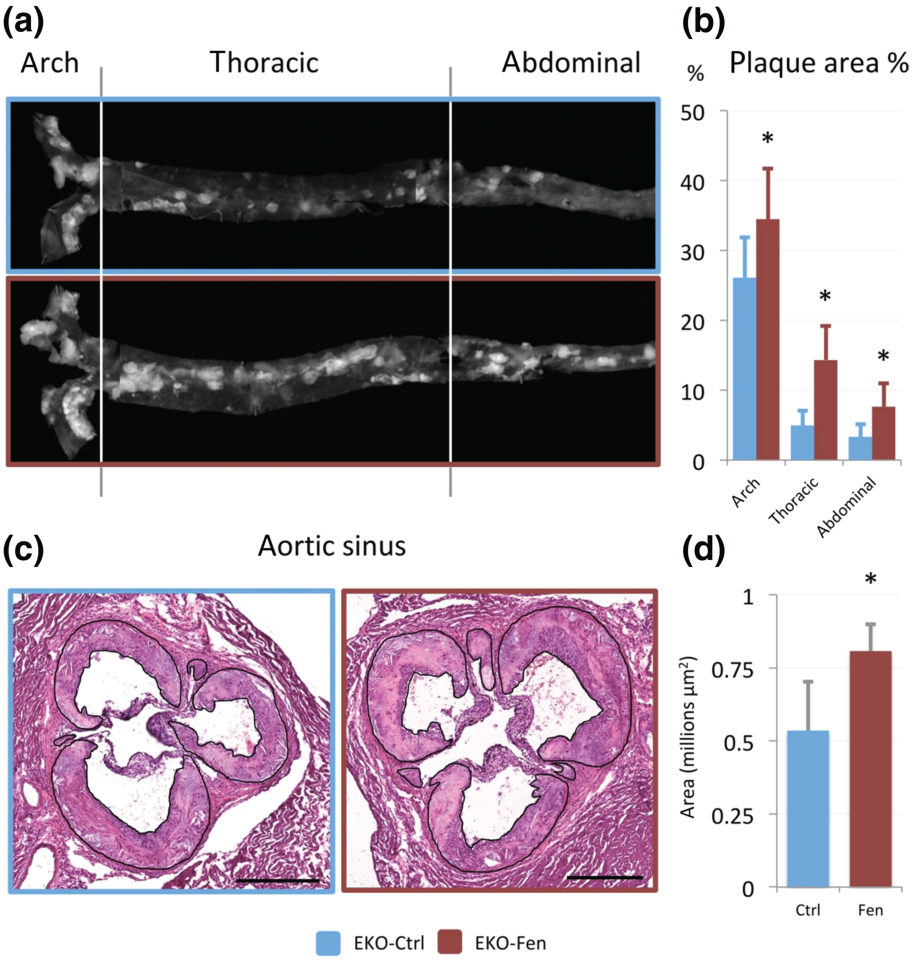

FIGURE 5 Representative image of aortas prepared with the en face method (a). The aorta (n = 20 per group) was cut lengthwise and pinned flat onto a black wax surface, and then the exposed plaques were quantified as a percentage of the whole aortic area (b). Representative H&E photomicrographs of aortic sinuses (n = 20 per group, c). Plaque extent is reported as square micrometres (d). Statistically significant differences were determined by unpaired two-tailed Student's t-test. *P < 0.05. Data are expressed as mean ± SD. Bar length = 500 µm

TABLE 1 Plaque size and composition in the aortic sinus of EKO-Ctrl and EKO-Fen mice

	Absolute values (mm^2)			% Total plaque area		
	EKO-Ctrl	EKO-Fen	P value	EKO-Ctrl	EKO-Fen	P value
Plaque area	0.535 ± 0.092	0.807 ± 0.168	**<0.05**	–	–	
Collagen area	0.241 ± 0.051	0.443 ± 0.097	<0.05	46.01 ± 10.08	54.31 ± 5.18	<0.05
Necrotic core area	0.103 ± 0.035	0.187 ± 0.057	<0.05	19.30 ± 6.28	23.12 ± 3.89	<0.05
Neutral lipids area	0.157 ± 0.065	0.141 ± 0.039	n.s.	28.75 ± 8.88	17.82 ± 4.38	<0.05
Foam cell area	0.188 ± 0.060	0.183 ± 0.059	n.s.	34.69 ± 7.59	22.57 ± 5.31	<0.05
Macrophage area	0.199 ± 0.047	0.190 ± 0.060	n.s.	36.89 ± 4.72	23.45 ± 5.84	<0.05

Atherosclerotic plaque area and areas occupied by collagen (Sirius Red staining), necrotic core, neutral lipids (ORO), foam cells and macrophages (anti-galectin-3 immunostaining) were quantified by two independent experimenters, blinded to the treatment, in aortic sinus sections (n = 20 per group). Results are presented as raw area number (in square millimetres, left) and as percentage of total plaque area (right). Statistically significant differences were determined by unpaired two-tailed Student's t-test. Data are shown as mean ± SD.

and hypochromic (MCHC −14.4%) compared with EKO-Ctrl. In WT mice, RBC were hypochromic (MCHC −3.5%) but no changes in the MCV were observed (Figure 6c).

Platelet counts were lower in treated mice compared with controls in both groups, but this decrease was significant only in EKO mice (−19.1%; Figure 6d).

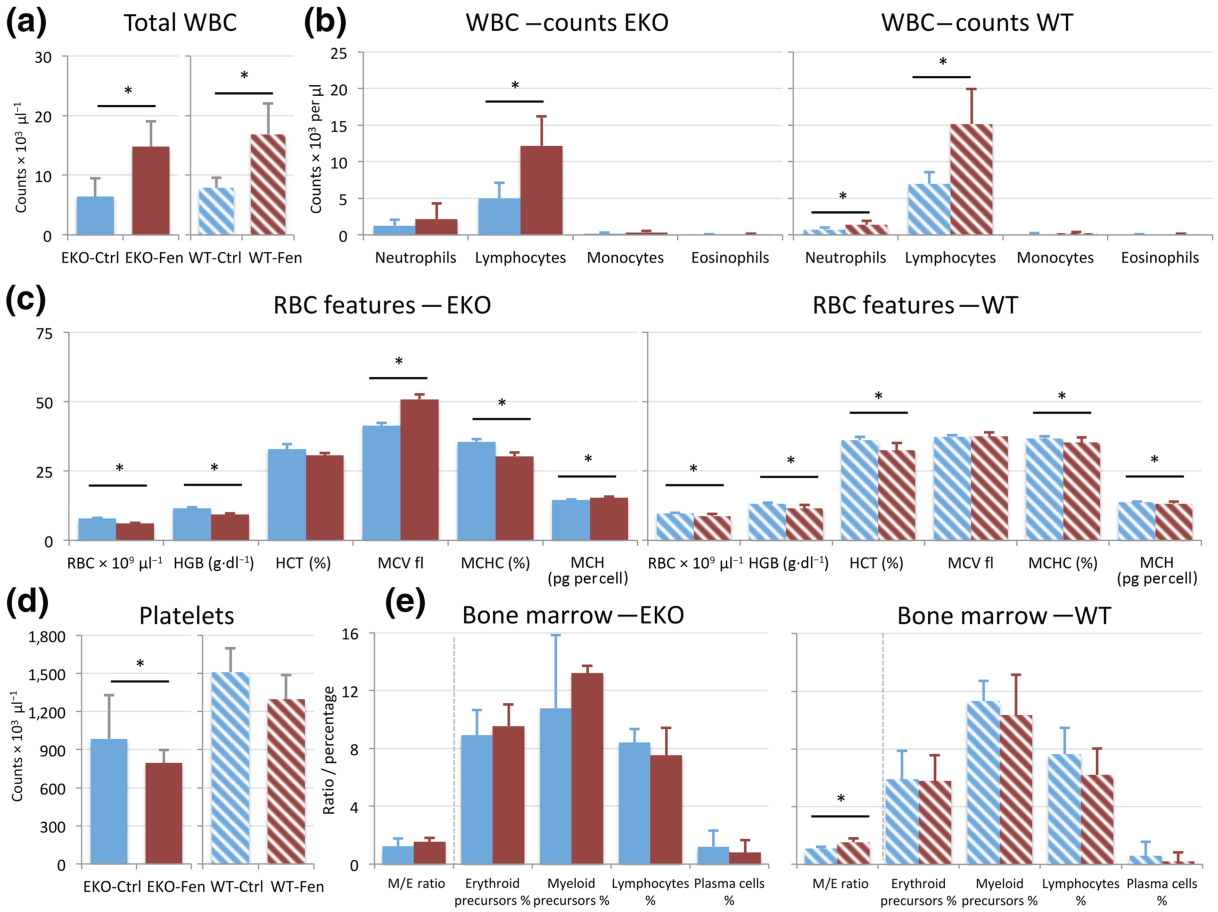

FIGURE 6 Cytologic evaluation of blood and bone marrow (n = 10 randomly chosen mice per group). RBC, red blood cells (erythrocyte number); WBC, white blood cells; HGB, Hb concentration; HCT, haematocrit; MCV, mean corpuscular volume; MCHC, mean corpuscular Hb concentration; MCH, mean corpuscular Hb; M/E ratio, monocyte to erythrocyte ratio. Statistically significant differences were determined by unpaired two-tailed Student's t-test. *P < 0.05. Data are expressed as mean ± SD

In bone marrow, an increase of the myeloid:erythroid ratio was found in both groups, but a significant difference was reached only in WT mice (+39.4%). No other significant difference was found, although in both groups, lymphocytes and plasma cells showed a moderate reduction in treated mice. The percentage of the proliferating pools of erythroid and myeloid cells was not significantly affected by treatment but showed an opposite trend in EKO and WT mice (Figure 6e).

3.6 | Immunophenotyping of blood, bone marrow and spleen

The increase of total counts of circulating leukocytes (CD45+) upon fenretinide treatment was further confirmed by flow cytometry in both EKO and WT mice (+67% and +139%, respectively, Figure 7a,d).

In EKO mice, this effect was mainly due to the rise of both T (CD3+) and B (CD19+) lymphocytes (Figure 7b). Within monocytes, fenretinide treatment in EKO also increased the relative amount of activated versus resting monocytes (Ly6C^{hi} versus Ly6C^{lo}; Figure 7c). In WT animals, fenretinide treatment caused a significant increase in all leukocyte subpopulations (Figure 7e).

The analysis of bone marrow did not unmask significant differences in the total count of leukocytes (CD45+/femur, Figure 7g) in both EKO and WT mice upon fenretinide treatment. However, the relative amount of myeloid cells (CD11b+) over the total leukocytes revealed an enrichment of this cell type in fenretinide treated animals of both mouse lines (Figure 7h). In addition, in EKO mice, fenretinide treatment significantly increased the relative amount of monocytes versus neutrophils (Figure 7i,j). No variations by treatment were instead observed in WT mice (Figure 7k).

In the spleen, absolute counts of myeloid cells (CD11b), dendritic cells, macrophages, T and B lymphocytes and consequently of total leukocytes were unaltered in EKO mice (Figure 7l,n). An increase of leukocyte subsets was instead overall observed in the spleen of WT mice that was significant for myeloid cells (+42.1%), dendritic cells (+74.7%), macrophages (+53.1%), B lymphocytes (+58.2) and total leukocytes (+48.9%; Figure 7m,o). When cellular count was corrected for spleen weight, the number of all main classes of leukocytes was significantly decreased in EKO mice (Figure 7 p,r: −54.9%, −48.3%, −52.9%, −60.8%, −60.9%, and −59.8% for myeloid, dendritic cells, macrophages, T and B lymphocytes, and total leukocytes, respectively), whereas no differences were detected in

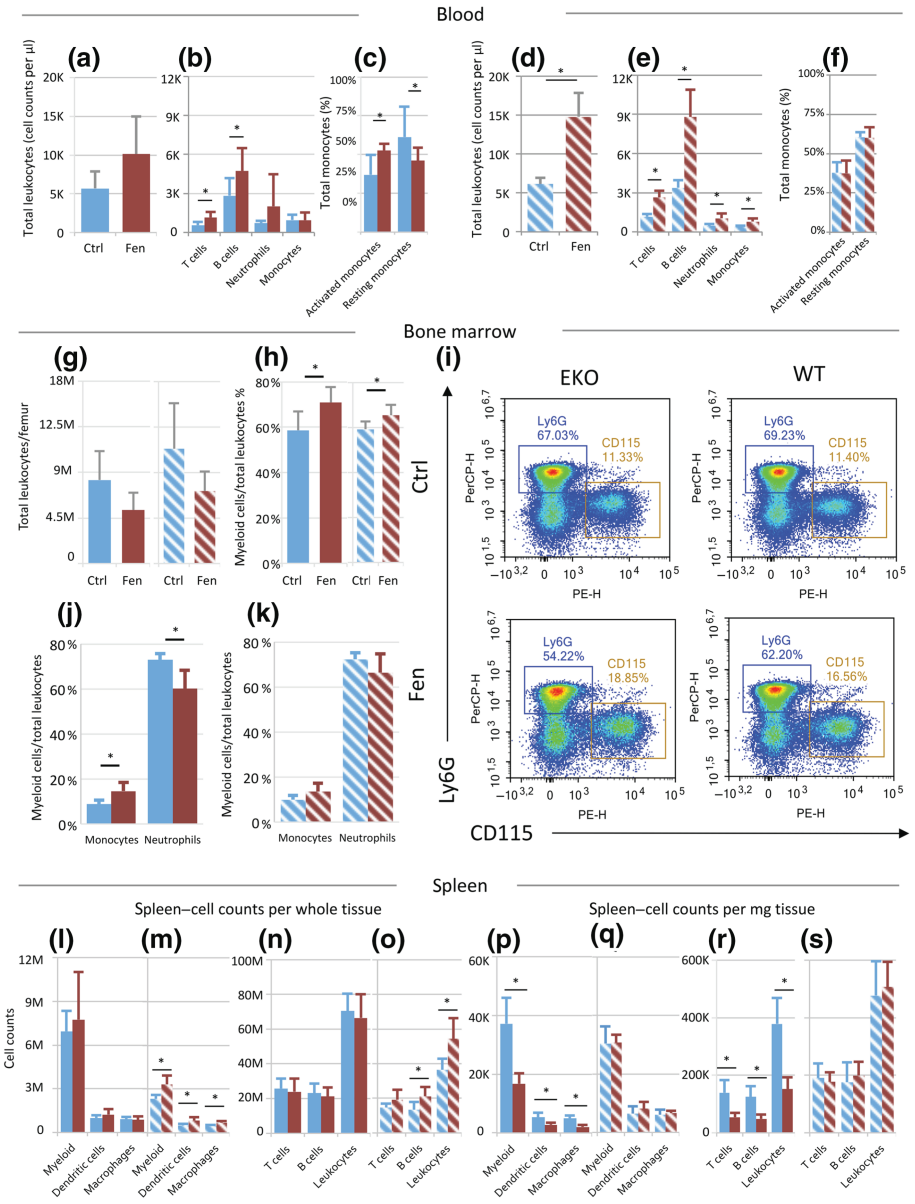

FIGURE 7 Flow cytofluorimetric evaluation of blood, bone marrow, and spleen (n = 5 randomly chosen mice per group). Total leukocyte count in the blood of EKO (a) and WT (d); count of T and B cells, neutrophils, and monocytes in the blood of EKO (b) and WT (e); percentage of activated (Ly6C^{hi}) and resting monocytes (Ly6C^{lo}) in the blood of EKO (c) and WT (f) is shown. Total count of leukocytes in the femur of EKO and WT mice (g); percentage of myeloid cells (CD11b+) on total leukocytes (h) and their subsets (j, k); representative dot plot from FACS analysis (i) is shown. Total count of spleen's immune cells in EKO (l, n) and WT (m, o); cell count corrected for spleen weight (mg) in EKO (p, r) and WT (q, s) is shown. Statistically significant differences were determined by unpaired two-tailed Student's t-test. *P < 0.05. Data are expressed as mean ± SD

WT mice (Figure 7q,s). These findings are in accordance with the morphological changes observed in both genotypes following fenretinide treatment. In WT mice, spleen weight was moderately increased (90 ± 20 mg and 120 ± 40 mg in WT-Ctrl and WT-Fen, respectively), whereas in EKO mice, the spleen appeared markedly enlarged (211 ± 67 mg and 597 ± 159 mg in EKO-Ctrl and EKO-Fen, respectively; Figure S1). In WT-Fen, histological examination showed an increased, although not significant, incidence of extramedullary haematopoiesis, characterized by the presence of haematopoietic cells expanding the red pulp (Table S2). On the contrary, in EKO-Fen mice compared to EKO-Ctrl mice, spleen parenchyma showed the presence of severe extramedullary haematopoiesis and a marked follicular atrophy (Table S5 and Figure 8a,b). Extramedullary haematopoiesis was also a constant finding in the liver of EKO-Fen (nine out of 10 animals), but not in that of EKO-Ctrl (one out of 10 mice; Figure 8c,d).

3.7 | Fenretinide increased erythrocyte destruction

Histological findings in kidney and liver indicated that fenretinide treatment to EKO mice accelerated erythrocyte turnover. In fact,

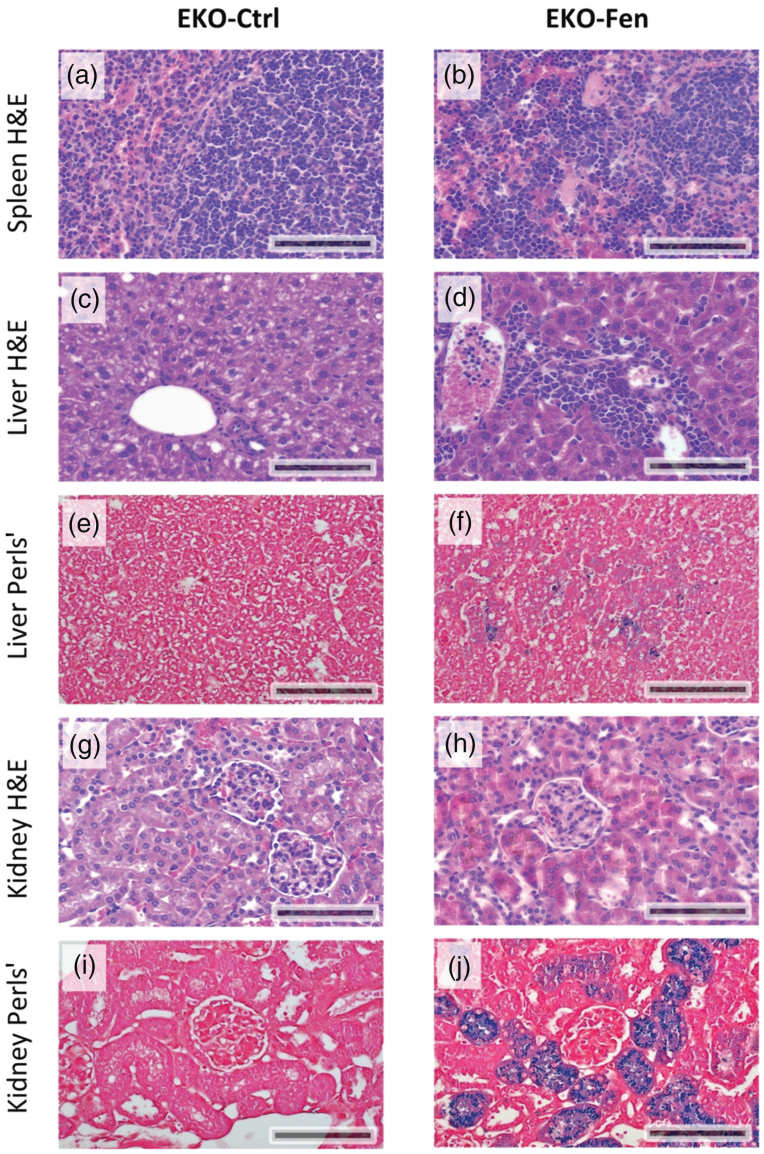

FIGURE 8 Spleen (H&E, a, b); extramedullary haematopoiesis expanding the red pulp mostly represented by erythroid cells: mild in EKO-Ctrl (a) with a large follicle on the right and severe in EKO-Fen (b) with an atrophic follicle on the right. Liver (H&E, c, d); extramedullary haematopoiesis: negative in EKO-Ctrl (c) and moderate in EKO-Fen expanding a portal area (d). Liver (Perls' iron stain, e, f); hemosiderin in the cytoplasm of Kupffer cells: negative in EKO-Ctrl (e) and moderate, multifocal presence in EKO-Fen (f). Kidney (H&E, g, h); hemosiderin, represented by granular brownish material, in the cytoplasm of proximal convoluted tubular epithelial cells: negative in EKO-Ctrl (g) and severe, multifocal presence in EKO-Fen (h). Kidney (Perls' iron stain, i, j); hemosiderin, represented by blue granules, in the cytoplasm of proximal convoluted tubular epithelial cells: negative in EKO-Ctrl (i) and severe, multifocal presence in EKO-fen (j). Bar length: 100 μm

hemosiderosis was absent in the kidney and liver of EKO-Ctrl and WT mice (Table S2), whereas in EKO-Fen the presence of hemosiderin was observed multifocally within the cytoplasm of tubular epithelial cells in the proximal convoluted tubules of the kidney in all animals (Figure 8 g–l and Table S6) and in the cytoplasm of Kupffer cells in the liver of 9 out of 10 mice (Figure 8e,f).

3.8 | Functional fibrinogen

A significant increase in the plasma fibrinogen activity was observed in EKO-Fen mice with respect to EKO-Ctrl (+48.7%; Figure S6). The same trend was observed in WT mice (+31.0%), although it did not reach statistical significance.

3.9 | Platelet/leukocyte aggregates

In total blood, the percentage of platelet-leukocyte aggregates was greater in EKO-Ctrl compared with WT-Ctrl mice (Figure S7A). This parameter was not modified by fenretinide treatment in WT mice, whereas it was strongly lowered in EKO animals, where it became comparable to that of WT mice (Figure S7A).

Remarkably, the analysis of leukocyte subsets showed that the percentage of monocyte and neutrophil–platelet aggregates was significantly higher in EKO-Ctrl versus WT-Ctrl mice (+112.81%) and fenretinide treatment only slightly modified these values, in both genotypes (Figure 9a).

When considering monocyte–platelet aggregates alone, untreated mice of both genotypes showed similar values (Figure 9b). Fenretinide tended to decrease the number of monocyte–platelet aggregates in WT mice (from 25.4 ± 7.2% to 15.1 ± 3.8%), whereas in EKO mice, the treatment significantly increased (43.3%) the number of aggregates (Figure 9b).

Finally, the percentage of circulating neutrophil–platelet aggregates was greater in EKO-Ctrl compared to WT-Ctrl mice. Fenretinide treatment did not cause any significant variation in the two genotypes (Figure S7B).

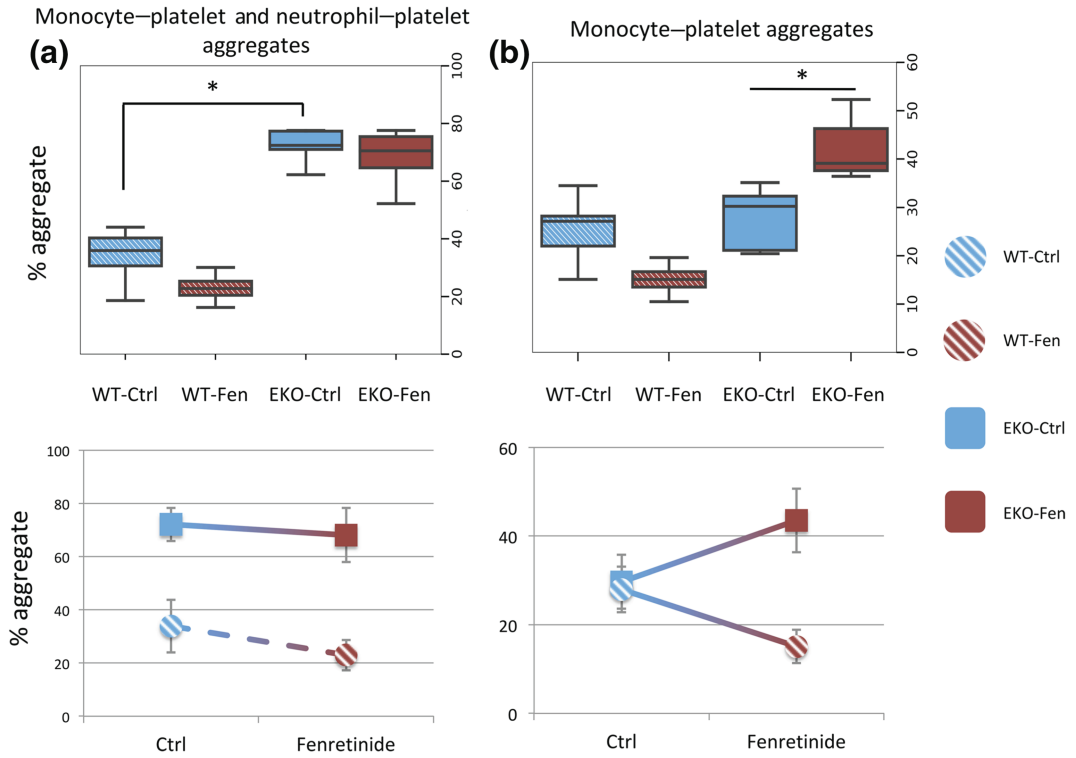

FIGURE 9 Flow cytometry analyses of percentage of (a) monocyte and neutrophil–platelet and (b) monocyte–platelet aggregates in whole blood of WT and EKO mice treated with or without fenretinide (n = 5 randomly chosen mice per group). In (a), aggregates in EKO-Ctrl were higher than both untreated groups, as well as aggregates in EKO-Fen were higher than both untreated groups. In (b), aggregates in WT-Fen were different from all EKO conditions. Fenretinide treatment resulted in significantly different aggregates in EKO. Statistically significant differences were determined by Kruskal–Wallis one-way ANOVA test, followed by Conover's post hoc test with Bonferroni P value adjustment method. *$P < 0.05$. Top: The upper and lower ends of the boxes indicate the 25th and 75th percentiles, respectively. The length of the box shows the interquartile range within which 50% of the values are located. The solid grey lines denote the median. Bottom: Data are expressed as mean ± SD

3.10 | Other histological findings

In the lungs, moderate to severe lesions characterized by the presence of foamy macrophages were a constant finding in EKO-Fen mice (Figure S8), whereas they were absent in EKO-Ctrl as well as in all WT animals (Table S2). Additionally, cholesterol crystals were occasionally observed only in EKO-Fen animals.

Morphological analysis did not show any significant difference between the skin of treated and untreated WT mice (Table S7). In both the experimental groups the epidermis appeared to have a build-up of ordinated overlapped layers of cells while in the dermis there were no signs of alteration. The presence of foam cells was detected only in treated and untreated EKO mice. Other morphological alterations were also visible, although shared almost equally in EKO-Ctrl and EKO-Fen animals (Table S7 and Figure S9).

4 | DISCUSSION

The main result of the present study is that, despite the favourable metabolic effects exerted by fenretinide treatment on glucose tolerance, fat mass accumulation, liver steatosis and, most importantly, on the plasma lipid levels, the treatment resulted into a surprising worsening of atherosclerosis. In this study, EKO mice were used as they spontaneously develop hypercholesterolaemia and atherosclerotic lesions that, like in humans, stem from early fatty streaks and develop into advanced and complex lesions (Nakashima, Plump, Raines, Breslow, & Ross, 1994; Plump et al., 1992). Only female EKO mice have been used because females develop atherosclerotic lesions at earlier age than males, resulting in a large differences (>50%) in plaque extent between sexes (Caligiuri, Nicoletti, Zhou, Törnberg, & Hansson, 1999). When fed on a high-fat diet lesion formation is greatly accelerated. Further, this dietary treatment also results in an impaired glucose metabolism (Nakashima et al., 1994; Su et al., 2006). Wild-type mice receiving the same treatments and diet were also included in the study to assess genotype-specific biases.

Fenretinide pharmacodynamics and toxicology have been known for a long time and a dietary formulation is possible (McCormick, Bagg, & Hultin, 1987; Preitner et al., 2009; Slawin et al., 1993). A formulation of 1-mg fenretinide per gram of diet has been chosen as proof-of-principle. A long-term treatment (12 weeks) has already been documented in diet-induced obese mice fed with high-fat diet supplemented with the selected fenretinide dosage (0.1% w/w) and even longer treatment times have been used (Preitner et al., 2009). As a readout of the

treatment the hepatic expression of Cyp26a1, a cytochrome involved in the metabolism of retinoids, was up-regulated fourfold in the liver of fenretinide-treated mice (Figure 3b).

The possible effects of fenretinide treatment on body weight, fat mass accumulation, glucose metabolism and plasma lipid levels, which has yet to be tested in the EKO model, were investigated in the present study. The reduction of body weight gain following fenretinide treatment has been thoroughly documented in wild-type and in genetically obese mice (Koh et al., 2012; Mcilroy et al., 2013; Preitner et al., 2009; Shearer et al., 2015). Consistent with these findings, in the present study fenretinide treatment was found to reduce body weight gain and fat mass in both EKO and wild-type mice. This mainly occurs via the inhibition of adipogenesis through prevention of C/EBPβ transcription (Mcilroy et al., 2016). The treatment was not expected to alter the food intake (Shearer et al., 2015) and, indeed, food intake was unchanged in EKO and negligibly increased in WT mice.

It has also been demonstrated how fenretinide causes insulin-sensitizing and antidiabetic effects in mice and overweight humans (Bikman et al., 2012). Reportedly, the inhibition of ceramide pathway biosynthesis enhances insulin sensitivity (Aerts et al., 2007) and fenretinide has been found to be inhibiting dihydroceramide desaturases, which catalyse the final step in *de novo* ceramide synthesis (Rahmaniyan, Curley, Obeid, Hannun, & Kraveka, 2011). Likewise, in the present study, fenretinide treatment resulted in significantly lower basal glycaemia in treated versus untreated EKO mice. Furthermore, throughout the whole glucose tolerance test treated EKO mice always showed average glucose levels trending towards 10–20% lower values than untreated mice. Slc2a4 (GLUT4) expression levels correlate with whole-body insulin-mediated glucose homeostasis (Atkinson, Griesel, King, Josey, & Olson, 2013). Moreover, insulin-resistant glucose transport in adipocytes from obese and diabetic subjects correlates with reduced GLUT4 expression (Berger et al., 1989). Accordingly, we found that Slc2a4 expression was almost twofold higher in the WAT of EKO-Fen, with respect to controls.

In mice, the main source of resistin (Retn gene) is white adipose tissue (Jamaluddin, Weakley, Yao, & Chen, 2012). Even if resistin was first described as a factor contributing to the development of insulin resistance and diabetes in humans, there is no clear consensus yet regarding its exact contribution to obesity and insulin sensitivity. However, resistin serum levels are positively associated with increased acute coronary syndrome (Jamaluddin et al., 2012). Further, several studies support a positive correlation between elevated serum resistin and obesity or impaired glucose tolerance (Luo et al., 2012; Malo et al., 2011). We found that Retn gene expression in WAT was decreased, almost by fivefold in EKO-Fen with respect to EKO-Ctrl.

Another reported beneficial effect of fenretinide treatment is the reduction of plasma lipids, including total cholesterol, triglycerides and free fatty acids in obese mice fed a high-fat diet (Koh et al., 2012). This holds true also in EKO mice, where fenretinide was able to dramatically and significantly reduce total cholesterol (−20.2%), triglycerides (−66.9%), and phospholipids (−20.1%). No relevant variations in the expression of genes involved in lipid metabolism were found, except for a threefold increase of Hmgcr, the rate-limiting enzyme in cholesterol synthesis. Additionally, hepatic steatosis and glycogen accumulation, typically observed in EKO mice on high-fat diet were greatly reduced by treatment.

Given the wealth of favourable preliminary data, the main objective of the present study was the evaluation of a possible effect of fenretinide on atherosclerosis development. Strikingly, and in apparent contrast with the data discussed above, the treatment resulted in a marked increase in the extent of atherosclerotic lesions in all aortic districts, including the aortic sinus. The larger necrotic core and the increased collagen deposition found in plaques of treated mice suggest that fenretinide accelerates plaque development, resulting in the presence of more advanced lesions. This result may not be explainable taking into account the data reviewed so far, especially considering the reduction of plasma lipid levels. While it is true that there was a remarkable absolute reduction of total cholesterol ($-229\ mg{\cdot}dl^{-1}$), plasma cholesterol levels remained very high, a characteristic feature of this mouse model. Nonetheless, this reduction in the lipid levels, however limited, should be paralleled by a reduced plaque development (Parolini et al., 2017).

The most remarkable macroscopic feature of EKO mice treated with fenretinide was an abnormally enlarged spleen. Also in WT mice the treatment resulted in significantly heavier spleens, although this variation was less dramatic. Whereas in WT mice this weight increase was paralleled by an increase in the leukocyte content, while in EKO mice the augmented organ mass was not associated with a change of total leukocyte number or individual leukocyte subpopulations. In fact these effects were the same in treated and untreated EKO mice. The histological analysis supported these findings, being the spleen of treated EKO mice characterized by small and atrophic follicles. Extramedullary haematopoiesis was detected in fenretinide treated WT mice as well as EKO mice. In these latter, the red pulp was strongly expanded, thus explaining, at least in part, the enlargement of this organ. Only in EKO-treated mice, extramedullary haematopoiesis was observed also in the liver.

Blood cytology analysis showed that in both EKO and WT mice the treatment induced a decrease of the erythroid mass. This decrease seemed to be due to a reduced production of RBC in WT mice, which had a normocytic hypochromic pattern. Conversely, in EKO mice, the macrocytic hypochromic pattern was consistent with active bone marrow regeneration, generally associated to blood loss or haemolysis. Histopathological findings strongly supported this latter hypothesis, as in the kidney as well as the hepatic Kupffer cells there was a massive deposition of hemosiderin pigment coming from disintegrating erythrocytes. Erythrolysis was a condition found only in EKO mice and possibly consequent to the severe hypercholesterolaemia that has been shown to increase the osmotic fragility of RBC (Fessler, Rose, Zhang, Jaramillo, & Zeldin, 2013). In addition, fenretinide treatment is associated to an augmented ROS production (Cuperus, Leen, Tytgat, Caron, & van Kuilenburg, 2010), which in turn reduces RBC deformability (Diederich et al., 2018). These two effects are synergized in EKO-Fen only, leading to peripheral haemolysis.

Fenretinide treatment caused a dramatic increase of circulating leukocytes in both WT and EKO mice. All leukocyte classes

contributed to this rise, with lymphocytes playing the major role. A similar response to fenretinide treatment has been recently reported in wild-type mice receiving higher doses of the drug (Cook et al., 2018). As fenretinide has only been tested in the clinic for the treatment of solid and blood malignancies it is difficult to translate this finding in humans.

Platelet counts were lower in EKO compared to WT mice. In EKO, however, large platelet clumps were frequently found in blood, suggesting that this decrease is likely due to a hyperactivation of platelets. Fenretinide treatment lowered platelet counts in both genotypes, although this trend was particularly severe, and statistically significant, only in EKO mice.

The haematological alterations discussed above, consequent to fenretinide treatment could, at least partially, explain the atherosclerosis worsening observed in EKO mice. Fenretinide treatment was not associated with increased erythrocytes accumulation within plaques, indicating that the accelerated atherosclerosis was not the result of a direct RBC accumulation, a known pro-atherogenic stimulus (Kolodgie et al., 2003).

Instead, we hypothesized that the atherosclerosis worsening could be the result of the peripheral destruction of erythrocytes observed in EKO treated mice, which has been reported to release inflammatory mediators resulting in a state of general inflammation (Randolph, 2009). Additionally, the percentage of circulating activated monocytes was increased by treatment. Monocytes are the primary inflammatory cell type that infiltrates early atherosclerotic plaques and their recruitment drives disease progression (Randolph, 2009). Interestingly, FACS analyses revealed an increase in the bone marrow of myeloid lineage cells with an imbalance towards monocyte versus neutrophil populations. Of note, increased bone marrow myelopoiesis and extramedullary myelopoiesis have been positively associated with atherosclerosis (Murphy et al., 2011; Yvan-Charvet et al., 2010). In addition, our observation that circulating activated monocytes are increased in treated EKO further links the immunomodulation induced by fenretinide to atherosclerosis development. Cytokine/chemokine evaluation in plasma and aorta confirmed that fenretinide treatment generated a pro-atherogenic inflammatory milieu. Specifically, the increased expression of Tnf and Ccl2 in EKO-Fen may have contributed to the continuous recruitment of monocytes from the bloodstream into the plaque, ultimately contributing to accelerated atherosclerosis progression. It can be hypothesized that an accelerated apoptosis or a defective efferocytosis of infiltrating macrophages may have contributed to the larger necrotic core observed in the atherosclerotic plaques of EKO-Fen, thus resulting in comparable amounts of macrophages in EKO-Fen and EKO-Ctrl.

Further, the greater percentage of monocyte/platelet aggregates detected in treated EKO mice might contribute to the marked atherosclerosis in these mice. Indeed, activated platelets bound circulating monocytes, promoting atherosclerotic plaque formation and development (Huo et al., 2003). In particular, both activated platelets and platelet–monocyte aggregates induce the adhesion of leukocytes to the endothelium, the recruitment of monocytes in atherosclerotic lesion and they increase cholesteryl ester accumulation in monocyte-derived macrophages, as well as the differentiation of CD34+ myeloid cells into foam cells (Daub et al., 2006).

Finally, the increased fibrinogen activity in EKO mice treated with fenretinide and the greater concomitant increase in atherosclerosis are consistent with data obtained in various epidemiological studies and animal models (Handa et al., 1989; Koopman et al., 1997; Uner et al., 2018). Interestingly, structures resembling Lambl's excrescences, filiform fronds originating from small thrombi, were identified uniquely in a subset of fenretinide-treated mice. This observation further supports the hypothesis of a pro-atherogenic effect of fenretinide occurring through endothelial damage, platelet and immune system activation.

In conclusion, all the above evidence demonstrate that fenretinide treatment, in spite of positive metabolic effects, severely altered blood cell turnover resulting in a worsening of atherosclerosis development in the main atherosclerosis-prone mouse model (Emini Veseli et al., 2017). Even if further investigations are required to demonstrate to what extent the above can be translated into the human setting, these results strongly suggest that careful selection and monitoring of patients undergoing fenretinide treatment is needed.

ACKNOWLEDGEMENTS

This work was funded by the European Community's Seventh Framework Programme (FP7/2012–2017) RiskyCAD, Grant 305739 (G.C.), by Fondazione CARIPLO (2011–0645) (G.C.), and by grants from MIUR Progetto Eccellenza. We are grateful to Ms. Elda Desiderio Pinto for administrative assistance. We deeply thank Elena Olmastroni for advices and checks on statistical analyses, and we thank Dr. Cinzia Parolini for technical support. Part of this work was carried out at NOLIMITS, an advanced imaging facility established by the Università degli Studi di Milano. Dr. Leonardo Sandrini is supported by the 32nd cycle PhD programme in "Scienze farmacologiche sperimentali e cliniche," Università degli Studi di Milano.

AUTHOR CONTRIBUTIONS

M.B., S.M., and G.C. conceived and managed the study. M.B. and S.M. wrote the paper. M.B. evaluated atherosclerosis development. S.M. performed molecular biology experiments and statistical analyses. F. B. performed FACS experiments. S.S. and E.S. performed extensive histological analyses. S.S.B., P.A., and L.S. assayed leukocyte–platelet interactions and assayed functional fibrinogen. F.A. and E.D. performed skin histology. R.L. helped conceiving the study and proofread the manuscript. S.P. performed extensive haematological analyses and bone marrow cytology. G.C. raised funds for the study, supervised all experiments, and critically revised the manuscript.

CONFLICT OF INTEREST

The authors declare no conflicts of interest.

DECLARATION OF TRANSPARENCY AND SCIENTIFIC RIGOUR

This Declaration acknowledges that this paper adheres to the principles for transparent reporting and scientific rigour of preclinical research as stated in the *BJP* guidelines for Design & Analysis, Immunoblotting and Immunochemistry, and Animal Experimentation, and as recommended by funding agencies, publishers and other organisations engaged with supporting research.

ORCID

Marco Busnelli https://orcid.org/0000-0003-3245-2872
Stefano Manzini https://orcid.org/0000-0002-1232-2635
Giulia Chiesa https://orcid.org/0000-0001-5553-1210

REFERENCES

Aburasayn, H., Al Batran, R., & Ussher, J. R. (2016). Targeting ceramide metabolism in obesity. *American Journal of Physiology. Endocrinology and Metabolism*[Online], *311*(2), E423–E435. Available from: http://www.ncbi.nlm.nih.gov/pubmed/27382035

Aerts, J. M., Ottenhoff, R., Powlson, A. S., Grefhorst, A., van Eijk, M., Dubbelhuis, P. F., … Overkleeft, H. S. (2007). Pharmacological inhibition of glucosylceramide synthase enhances insulin sensitivity. *Diabetes*[Online], *56*(5), 1341–1349. Available from: http://www.ncbi.nlm.nih.gov/pubmed/17287460

Alexander, S. P., Christopoulos, A., Davenport, A. P., Kelly, E., Marrion, N. V., Peters, J. A., et al. (2017). The Concise Guide to PHARMACOLOGY 2017/18: G protein-coupled receptors. *British Journal of Pharmacology*, *174*(Suppl 1), S17–S129.

Alexander, S. P., Fabbro, D., Kelly, E., Marrion, N. V., Peters, J. A., Faccenda, E., et al. (2017). The Concise Guide to PHARMACOLOGY 2017/18: Enzymes. *British Journal of Pharmacology*, *174*(Suppl 1), S272–S359.

Alexander, S. P. H., Roberts, R. E., Broughton, B. R. S., Sobey, C. G., George, C. H., Stanford, S. C., … Ahluwalia, A. (2018). Goals and practicalities of immunoblotting and immunohistochemistry: A guide for submission to the *British Journal of Pharmacology*. *British Journal of Pharmacology*[Online], *175*(3), 407–411. Available from: http://www.ncbi.nlm.nih.gov/pubmed/29350411

Amadio, P., Colombo, G. I., Tarantino, E., Gianellini, S., Ieraci, A., Brioschi, M., … Barbieri, S. S. (2017). BDNFVal66met polymorphism: A potential bridge between depression and thrombosis. *European Heart Journal*[Online], *38*(18), 1426–1435. Available from: http://www.ncbi.nlm.nih.gov/pubmed/26705390

Amadio, P., Tarantino, E., Sandrini, L., Tremoli, E., & Barbieri, S. S. (2017). Prostaglandin-endoperoxide synthase-2 deletion affects the natural trafficking of annexin A2 in monocytes and favours venous thrombosis in mice. *Thrombosis and Haemostasis*[Online], *117*(8), 1486–1497. Available from: http://www.ncbi.nlm.nih.gov/pubmed/28536720

Arnaboldi, F., Busnelli, M., Cornaghi, L., Manzini, S., Parolini, C., Dellera, F., … Chiesa, G. (2015). High-density lipoprotein deficiency in genetically modified mice deeply affects skin morphology: A structural and ultrastructural study. *Experimental Cell Research*[Online], *338*(1), 105–112. Available from: http://www.ncbi.nlm.nih.gov/pubmed/26241937

Atkinson, B. J., Griesel, B. A., King, C. D., Josey, M. A., & Olson, A. L. (2013). Moderate glut4 overexpression improves insulin sensitivity and fasting triglyceridemia in high-fat diet-fed transgenic mice. *Diabetes*, *62*(7), 2249–2258.

Berger, J., Biswas, C., Vicario, P. P., Strout, H. V., Saperstein, R., & Pilch, P. F. (1989). Decreased expression of the insulin-responsive glucose transporter in diabetes and fasting. *Nature*[Online], *340*(6228), 70–72. Available from: http://www.ncbi.nlm.nih.gov/pubmed/2739728

Berry, D. C., DeSantis, D., Soltanian, H., Croniger, C. M., & Noy, N. (2012). Retinoic acid upregulates preadipocyte genes to block adipogenesis and suppress diet-induced obesity. *Diabetes*[Online], *61*(5), 1112–1121. Available from: http://www.ncbi.nlm.nih.gov/pubmed/22396202

Berry, D. C., & Noy, N. (2009). All-*trans*-retinoic acid represses obesity and insulin resistance by activating both peroxisome proliferation-activated receptor β/δ and retinoic acid receptor. *Molecular and Cellular Biology*[Online], *29*(12), 3286–3296. Available from: http://www.ncbi.nlm.nih.gov/pubmed/19364826

Bikman, B. T., Guan, Y., Shui, G., Siddique, M. M., Holland, W. L., Kim, J. Y., … Summers, S. A. (2012). Fenretinide prevents lipid-induced insulin resistance by blocking ceramide biosynthesis. *The Journal of Biological Chemistry*[Online], *287*(21), 17426–17437. Available from: http://www.ncbi.nlm.nih.gov/pubmed/22474281

Busnelli, M., Manzini, S., Hilvo, M., Parolini, C., Ganzetti, G. S., Dellera, F., … Chiesa, G. (2017). Liver-specific deletion of the Plpp3 gene alters plasma lipid composition and worsens atherosclerosis in apoE$^{-/-}$ mice. *Scientific Reports*[Online], *7*, 44503. Available from: http://www.nature.com/articles/srep44503

Caligiuri, G., Nicoletti, A., Zhou, X., Törnberg, I., & Hansson, G. K. (1999). Effects of sex and age on atherosclerosis and autoimmunity in apoE-deficient mice. *Atherosclerosis*[Online], *145*(2), 301–308. Available from: http://www.ncbi.nlm.nih.gov/pubmed/10488957

Cook, J. C., Obert, L. A., Koza-Taylor, P., Coskran, T. M., Opsahl, A. C., Ziemek, D., … Criswell, K. A. (2018). From the cover: Fenretinide, troglitazone, and elmiron add to weight of evidence support for hemangiosarcoma mode-of-action from studies in mice. *Toxicological Sciences: An Official Journal of the Society of Toxicology*[Online], *161*(1), 58–75. Available from: http://www.ncbi.nlm.nih.gov/pubmed/28973697

Cooper, J. P., Reynolds, C. P., Cho, H., & Kang, M. H. (2017). Clinical development of fenretinide as an antineoplastic drug: Pharmacology perspectives. *Experimental Biology and Medicine (Maywood, N.J.)*[Online], *242*(11), 1178–1184. Available from: http://www.ncbi.nlm.nih.gov/pubmed/28429653

Cuperus, R., Leen, R., Tytgat, G. A. M., Caron, H. N., & van Kuilenburg, A. B. P. (2010). Fenretinide induces mitochondrial ROS and inhibits the mitochondrial respiratory chain in neuroblastoma. *Cellular and Molecular Life Sciences: CMLS*[Online], *67*(5), 807–816. Available from: http://www.ncbi.nlm.nih.gov/pubmed/19941060

Curtis, M. J., Bond, R. A., Spina, D., Ahluwalia, A., Alexander, S. P. A., Giembycz, M. A., … McGrath, J. C. (2015). Experimental design and analysis and their reporting: New guidance for publication in *BJP*. *British Journal of Pharmacology*[Online], *172*(14), 3461–3471. Available from: http://www.ncbi.nlm.nih.gov/pubmed/26114403

Daub, K., Langer, H., Seizer, P., Stellos, K., May, A. E., Goyal, P., … Gawaz, M. (2006). Platelets induce differentiation of human CD34+ progenitor cells into foam cells and endothelial cells. *FASEB Journal: Official Publication of the Federation of American Societies for Experimental Biology*[Online], *20*(14), 2559–2561. Available from: http://www.ncbi.nlm.nih.gov/pubmed/17077283

Diederich, L., Suvorava, T., Sansone, R., Keller, T. C. S., Barbarino, F., Sutton, T. R., … Cortese-Krott, M. M. (2018). On the effects of reactive oxygen species and nitric oxide on red blood cell deformability. *Frontiers in Physiology*[Online], *9*, 332. Available from: http://www.ncbi.nlm.nih.gov/pubmed/29867516

Emini Veseli, B., Perrotta, P., De Meyer, G. R. A., Roth, L., Van der Donckt, C., Martinet, W., & De Meyer, G. R. Y. (2017). Animal models of

atherosclerosis. *European Journal of Pharmacology*[Online], *816*(April), 3–13. Available from: https://doi.org/10.1016/j.ejphar.2017.05.010

Fessler, M. B., Rose, K., Zhang, Y., Jaramillo, R., & Zeldin, D. C. (2013). Relationship between serum cholesterol and indices of erythrocytes and platelets in the US population. *Journal of Lipid Research*[Online], *54* (11), 3177–3188. Available from: http://www.ncbi.nlm.nih.gov/pubmed/23999863

Handa, K., Kono, S., Saku, K., Sasaki, J., Kawano, T., Sasaki, Y., … Arakawa, K. (1989). Plasma fibrinogen levels as an independent indicator of severity of coronary atherosclerosis. *Atherosclerosis*[Online], *77*(2–3), 209–213. Available from: http://www.ncbi.nlm.nih.gov/pubmed/2751752

Harding, S. D., Sharman, J. L., Faccenda, E., Southan, C., Pawson, A. J., Ireland, S., et al. (2018). The IUPHAR/BPS Guide to PHARMACOLOGY in 2018: Updates and expansion to encompass the new guide to immunopharmacology. *Nucleic Acids Research*, *46*(D1), D1091–D1106.

Howard, S. R., Oleari, R., Poliandri, A., Chantzara, V., Fantin, A., Ruiz-Babot, G., … Dunkel, L. (2018). *HS6ST1* insufficiency causes self-limited delayed puberty in contrast with other GnRH deficiency genes. *The Journal of Clinical Endocrinology and Metabolism*[Online], *103*(9), 3420–3429. Available from: http://www.ncbi.nlm.nih.gov/pubmed/29931354

Huo, Y., Schober, A., Forlow, S. B., Smith, D. F., Hyman, M. C., Jung, S., … Ley, K. (2003). Circulating activated platelets exacerbate atherosclerosis in mice deficient in apolipoprotein E. *Nature Medicine*[Online], *9*(1), 61–67. Available from: http://www.ncbi.nlm.nih.gov/pubmed/12483207

Jamaluddin, M. S., Weakley, S. M., Yao, Q., & Chen, C. (2012). Resistin: Functional roles and therapeutic considerations for cardiovascular disease. *British Journal of Pharmacology*[Online], *165*(3), 622–632. Available from: http://www.ncbi.nlm.nih.gov/pubmed/21545576

Kilkenny, C., Browne, W., Cuthill, I. C., Emerson, M., & Altman, D. G. (2010). Animal research: Reporting in vivo experiments: The ARRIVE guidelines. *British Journal of Pharmacology*, *160*, 1577–1579.

Koh, I., Jun, H.-S., Choi, J. S., Lim, J. H., Kim, W. H., Yoon, J. B., & Song, J. (2012). Fenretinide ameliorates insulin resistance and fatty liver in obese mice. *Biological & Pharmaceutical Bulletin*[Online], *35*(3), 369–375. Available from: http://joi.jlc.jst.go.jp/JST.JSTAGE/bpb/35.369?from=CrossRef.

Kolodgie, F. D., Gold, H. K., Burke, A. P., Fowler, D. R., Kruth, H. S., Weber, D. K., … Virmani, R. (2003). Intraplaque hemorrhage and progression of coronary atheroma. *The New England Journal of Medicine*[Online], *349* (24), 2316–2325. Available from: http://www.ncbi.nlm.nih.gov/pubmed/14668457

Koopman, J., Maas, A., Rezaee, F., Havekes, L., Verheijen, J., Gijbels, M., & Haverkate, F. (1997). Fibrinogen and atherosclerosis: A study in transgenic mice. *Fibrinolysis and Proteolysis*[Online], *11*, 19–21. Available from: https://linkinghub.elsevier.com/retrieve/pii/S0268949997800161.

Lachance, C., Wojewodka, G., Skinner, T. A. A. A., Guilbault, C., De Sanctis, J. B., & Radzioch, D. (2013). Fenretinide corrects the imbalance between Ω-6 to Ω-3 polyunsaturated fatty acids and inhibits macrophage inflammatory mediators via the ERK pathway. *PLoS ONE* [Online], *8*(9), e74875. Available from: https://doi.org/10.1016/j.phrs.2018.12.022

Livak, K. J., & Schmittgen, T. D. (2001). Analysis of relative gene expression data using real-time quantitative PCR and the $2^{-\Delta\Delta C_T}$ method. *Methods (San Diego, Calif.)*[Online], *25*(4), 402–408. Available from: http://www.ncbi.nlm.nih.gov/pubmed/11846609

Luo, R., Li, X., Jiang, R., Gao, X., Lü, Z., & Hua, W. (2012). Serum concentrations of resistin and adiponectin and their relationship to insulin resistance in subjects with impaired glucose tolerance. *The Journal of International Medical Research*[Online], *40*(2), 621–630. Available from: http://www.ncbi.nlm.nih.gov/pubmed/22613423

Mackie, I. J., Kitchen, S., Machin, S. J., Lowe, G. D. O., & Haemostasis and Thrombosis Task Force of the British Committee for Standards in Haematology (2003). Guidelines on fibrinogen assays. *British Journal of Haematology*[Online], *121*(3), 396–404. Available from: http://www.ncbi.nlm.nih.gov/pubmed/12716362

Malo, E., Ukkola, O., Jokela, M., Moilanen, L., Kähönen, M., Nieminen, M. S., … Kesäniemi, Y. A. (2011). Resistin is an indicator of the metabolic syndrome according to five different definitions in the Finnish Health 2000 survey. *Metabolic Syndrome and Related Disorders*[Online], *9*(3), 203–210. Available from: http://www.liebertonline.com/doi/abs/10.1089/met.2010.0106

Manzini, S., Busnelli, M., Parolini, C., Minoli, L., Ossoli, A., Brambilla, E., … Chiesa, G. (2018). Topiramate protects apoE-deficient mice from kidney damage without affecting plasma lipids. *Pharmacological Research* [Online], *141*(9), 189–200. Available from: https://doi.org/10.1016/j.phrs.2018.12.022

Manzini, S., Pinna, C., Busnelli, M., Cinquanta, P., Rigamonti, E., Ganzetti, G. S., … Chiesa, G. (2015). β2-adrenergic activity modulates vascular tone regulation in lecithin:cholesterol acyltransferase knockout mice. *Vascular Pharmacology*[Online], *74*, 114–121. Available from: http://www.ncbi.nlm.nih.gov/pubmed/26254103

Marchesi, M., Parolini, C., Caligari, S., Gilio, D., Manzini, S., Busnelli, M., … Chiesa, G. (2011). Rosuvastatin does not affect human apolipoprotein A-I expression in genetically modified mice: A clue to the disputed effect of statins on HDL. *British Journal of Pharmacology*[Online], *164* (5), 1460–1468. Available from: http://www.ncbi.nlm.nih.gov/pubmed/21486287

McCormick, D. L., Bagg, B. J., & Hultin, T. A. (1987). Comparative activity of dietary or topical exposure to three retinoids in the promotion of skin tumor induction in mice. *Cancer Research*[Online], *47*(22), 5989–5993. Available from: http://www.ncbi.nlm.nih.gov/pubmed/2959358

Mcilroy, G. D., Delibegovic, M., Owen, C., Stoney, P. N., Shearer, K. D., McCaffery, P. J., & Mody, N. (2013). Fenretinide treatment prevents diet-induced obesity in association with major alterations in retinoid homeostatic gene expression in adipose, liver, and hypothalamus. *Diabetes*[Online], *62*(3), 825–836. Available from: http://www.ncbi.nlm.nih.gov/pubmed/23193184

Mcilroy, G. D., Tammireddy, S. R., Maskrey, B. H., Grant, L., Doherty, M. K., Watson, D. G., … Mody, N. (2016). Fenretinide mediated retinoic acid receptor signalling and inhibition of ceramide biosynthesis regulates adipogenesis, lipid accumulation, mitochondrial function and nutrient stress signalling in adipocytes and adipose tissue. *Biochemical Pharmacology*[Online], *100*, 86–97. Available from: http://www.ncbi.nlm.nih.gov/pubmed/26592777

Mody, N., & Mcilroy, G. D. (2014). The mechanisms of fenretinide-mediated anti-cancer activity and prevention of obesity and type-2 diabetes. *Biochemical Pharmacology*[Online], *91*(3), 277–286. Available from: http://www.ncbi.nlm.nih.gov/pubmed/25069047

Murphy, A. J., Akhtari, M., Tolani, S., Pagler, T., Bijl, N., Kuo, C.-L., … Tall, A. R. (2011). ApoE regulates hematopoietic stem cell proliferation, monocytosis, and monocyte accumulation in atherosclerotic lesions in mice. *The Journal of Clinical Investigation*[Online], *121*(10), 4138–4149. Available from: http://www.ncbi.nlm.nih.gov/pubmed/21968112

Nakashima, Y., Plump, A. S., Raines, E. W., Breslow, J. L., & Ross, R. (1994). ApoE-deficient mice develop lesions of all phases of atherosclerosis throughout the arterial tree. *Arteriosclerosis and Thrombosis: A Journal*

of Vascular Biology[Online], *14*(1), 133–140. Available from: http://atvb.ahajournals.org/cgi/doi/10.1161/01.ATV.14.1.133

Parolini, C., Bjorndal, B., Busnelli, M., Manzini, S., Ganzetti, G. S., Dellera, F., … Chiesa, G. (2017). Effect of dietary components from Antarctic krill on atherosclerosis in apoE-deficient mice. *Molecular Nutrition & Food Research*[Online], *61*(12), 1700098. Available from: http://doi.wiley.com/10.1002/mnfr.201700098

Parolini, C., Busnelli, M., Ganzetti, G. S., Dellera, F., Manzini, S., Scanziani, E., … Chiesa, G. (2014). Magnetic resonance imaging visualization of vulnerable atherosclerotic plaques at the brachiocephalic artery of apolipoprotein E knockout mice by the blood-pool contrast agent B22956/1. *Molecular Imaging*[Online], *13*(5). Available from: http://www.ncbi.nlm.nih.gov/pubmed/24825406

Parolini, C., Vik, R., Busnelli, M., Bjørndal, B., Holm, S., Brattelid, T., … Chiesa, G. (2014). A salmon protein hydrolysate exerts lipid-independent anti-atherosclerotic activity in apoE-deficient mice. *PLoS ONE*[Online], *9*(5), e97598. Available from: http://www.ncbi.nlm.nih.gov/pubmed/24840793

Petersen, M. C., & Shulman, G. I. (2018). Mechanisms of insulin action and insulin resistance. *Physiological Reviews*[Online], *98*(4), 2133–2223. Available from: http://www.ncbi.nlm.nih.gov/pubmed/30067154

Plump, A. S., Smith, J. D., Hayek, T., Aalto-Setälä, K., Walsh, A., Verstuyft, J. G., … Breslow, J. L. (1992). Severe hypercholesterolemia and atherosclerosis in apolipoprotein E-deficient mice created by homologous recombination in ES cells. *Cell*[Online], *71*(2), 343–353. Available from: http://www.ncbi.nlm.nih.gov/pubmed/1423598

Pohlert, T. (2014). The pairwise multiple comparison of mean ranks package (PMCMR). [Online]. Available from: https://cran.r-project.org/package=PMCMR.

Preitner, F., Mody, N., Graham, T. E., Peroni, O. D., & Kahn, B. B. (2009). Long-term fenretinide treatment prevents high-fat diet-induced obesity, insulin resistance, and hepatic steatosis. *American Journal of Physiology. Endocrinology and Metabolism*[Online], *297*(6), E1420–E1429. Available from: http://ajpendo.physiology.org/cgi/doi/10.1152/ajpendo.00362.2009

R Core Team (2017). R: A language and environment for statistical computing. [Online]. Available from: https://www.r-project.org/.

Rahmaniyan, M., Curley, R. W., Obeid, L. M., Hannun, Y. A., & Kraveka, J. M. (2011). Identification of dihydroceramide desaturase as a direct in vitro target for fenretinide. *The Journal of Biological Chemistry*[Online], *286*(28), 24754–24764. Available from: http://www.ncbi.nlm.nih.gov/pubmed/21543327

Randolph, G. J. (2009). The fate of monocytes in atherosclerosis. *Journal of Thrombosis and Haemostasis: JTH*[Online], *7*(Suppl 1 (1)), 28–30. Available from: http://www.ncbi.nlm.nih.gov/pubmed/19630762

Sandrini, L., Ieraci, A., Amadio, P., Popoli, M., Tremoli, E., & Barbieri, S. S. (2017). Apocynin prevents abnormal megakaryopoiesis and platelet activation induced by chronic stress. *Oxidative Medicine and Cellular Longevity*, *2017*(7), 9258937.

Schneider, C. A., Rasband, W. S., & Eliceiri, K. W. (2012). NIH image to ImageJ: 25 years of image analysis. *Nature Methods*. [Online], *9*(7), 671–675. https://doi.org/10.1038/nmeth.2089

Shearer, K. D., Morrice, N., Henderson, C., Reekie, J., Mcilroy, G. D., McCaffery, P. J., … Mody, N. (2015). Fenretinide prevents obesity in aged female mice in association with increased retinoid and estrogen signaling. *Obesity (Silver Spring, Md.)*[Online], *23*(8), 1655–1662. Available from: http://www.ncbi.nlm.nih.gov/pubmed/26179846

Slawin, K., Kadmon, D., Park, S. H., Scardino, P. T., Anzano, M., Sporn, M. B., & Thompson, T. C. (1993). Dietary fenretinide, a synthetic retinoid, decreases the tumor incidence and the tumor mass of ras+*myc*-induced carcinomas in the mouse prostate reconstitution model system. *Cancer Research*[Online], *53*(19), 4461–4465. Available from: http://www.ncbi.nlm.nih.gov/pubmed/8402613

Su, Z., Li, Y., James, J. C., Matsumoto, A. H., Helm, G. A., Lusis, A. J., & Shi, W. (2006). Genetic linkage of hyperglycemia, body weight and serum amyloid-P in an intercross between C57BL/6 and C3H apolipoprotein E-deficient mice. *Human Molecular Genetics*[Online], *15*(10), 1650–1658. Available from: http://www.ncbi.nlm.nih.gov/pubmed/16595606

Uner, A. G., Unsal, C., Unsal, H., Erdogan, M. A., Koc, E., Ekici, M., … Tarin, L. (2018). Mice with diet-induced obesity demonstrate a relative prothrombotic factor profile and a thicker aorta with reduced ex-vivo function. *Blood Coagulation & Fibrinolysis: An International Journal in Haemostasis and Thrombosis*[Online], *29*(3), 257–266. Available from: http://www.ncbi.nlm.nih.gov/pubmed/29624513

Vik, R., Busnelli, M., Parolini, C., Bjørndal, B., Holm, S., Bohov, P., … Berge, R. K. (2013). An immunomodulating fatty acid analogue targeting mitochondria exerts anti-atherosclerotic effect beyond plasma cholesterol-lowering activity in apoE$^{-/-}$ mice. *PLoS ONE*[Online], *8*(12), e81963. Available from: http://www.ncbi.nlm.nih.gov/pubmed/24324736

Wickham, H. (2007). Reshaping data with the reshape package. *Journal of Statistical Software*[Online], *21*(12). Available from: http://www.jstatsoft.org/v21/i12/paper

Yvan-Charvet, L., Pagler, T., Gautier, E. L., Avagyan, S., Siry, R. L., Han, S., … Tall, A. R. (2010). ATP-binding cassette transporters and HDL suppress hematopoietic stem cell proliferation. *Science (New York, N.Y.)*[Online], *328*(5986), 1689–1693. Available from: http://www.ncbi.nlm.nih.gov/pubmed/20488992

Zizola, C. F., Frey, S. K., Jitngarmkusol, S., Kadereit, B., Yan, N., & Vogel, S. (2010). Cellular retinol-binding protein type I (CRBP-I) regulates adipogenesis. *Molecular and Cellular Biology*[Online], *30*(14), 3412–3420. Available from: http://www.ncbi.nlm.nih.gov/pubmed/20498279

SUPPORTING INFORMATION

Additional supporting information may be found online in the Supporting Information section at the end of the article.

How to cite this article: Busnelli M, Manzini S, Bonacina F, et al. Fenretinide treatment accelerates atherosclerosis development in apoE-deficient mice in spite of beneficial metabolic effects. *Br J Pharmacol*. 2019;1–18. https://doi.org/10.1111/bph.14869